



**MECHANICAL PROPERTIES OF FRICTION STIR WELDED
5083-H321 AND 6082-T651 DISSIMILAR ALUMINIUM
ALLOYS.**

by

Vuyani Moni

**Thesis submitted in fulfilment of the requirements for the
degree**

Master of Engineering in Mechanical Engineering

in the Faculty of Engineering and the Built Environment

at the Cape Peninsula University of Technology.

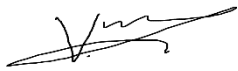
Supervisor: Dr V. Msomi

Bellville

Date submitted: June 2020

DECLARATION

I, Vuyani Moni, declare that the contents of this thesis represent my own unaided work, and that the thesis has not previously been submitted for academic examination towards any qualification. Furthermore, it represents my own opinions and not necessarily those of the Cape Peninsula University of Technology.



Vuyani Moni

11 June 2020

Date

ABSTRACT

Friction stir welding (FSW) is the fastest growing joining technique and the major prospective method of producing reliable welded components in a more efficient environmentally friendly manner. FSW relies on repeatability, integrity and easy of producing components that were impossible to produce before. This method is underpinned by the use of non-consumable tool, easy use of parameters to set for constant production and attainable tool geometries.

The aim of this project was to investigate mechanical properties of Friction Stir Welded 5083-H321 and 6082-T651 dissimilar aluminium alloys. Tool steel H13 tri-flat threaded tool was used with tool rotational speed of 800rpm and traverse speed of 60mm/min on a 6mm thick plates.

Plates were FS welded whereby 5083-H321 was placed on the advancing side and 6082-T651 on the retreating side and the plates were changed vice versa with the speeds kept unchanged. Specimen were extracted from different locations of FS welded joints being the start, middle and the end of the weld and the effect thereof was studied on the tensile strength, bending strength, microhardness, macrostructure, microstructure and scanning electron microscope. All the extracted specimens were compared to parent materials.

Plates were FS welded successfully with no surface voids observed on visual inspection and on internal metallurgical structures. Macrostructure showed similar patterns for advancing, retreating and locations of specimen regarding the orientation and nature of TMAZ, HAZ and SZ. However, the microstructures revealed more homogenous mixture of SZ when 5083-H321 was retreating. Grain sizes when 6082-T651 was advancing were bigger than when 5083-H321 was advancing though there was no positional significance noted. Average micro-hardness values were found to be better when 6082-T651 was advancing. The average size of micro-hardness values for 6082-T651 was 70HV while 5083-H321 was 60HV.

Tensile tests specimens broke on 6082-T651 HAZ for all the specimens. The 5083-H321 on advancing side had better UTS though 6082-T651 on advancing showed higher elongations. In bending tests, parent materials managed to achieve 180°bend without signs of cracks while the welded joints managed 90°bend and started cracking on the root welds along the butt interface.

Bending tests proved to have better strength than tensile tests for both parent materials and welded joints. Scanning electron microscope (SEM) fractograph was characterised by ductile dimples, micro-voids and shearing during tensile testing.

The study was found to be in congruence with most previous findings in many aspects. The only contradiction observed was the nugget pointing towards the advancing side when the 6082-T651 was on the retreating side, this was contrary to the most studies reviewed.

ACKNOWLEDGEMENTS

I would like to thank God Almighty for the strength to carry through this work. Through Him I can do all things.

I would like to acknowledge the following people who helped and encouraged me to complete this work:

- My supervisor Dr V Msomi, who through thick and thin made sure that I get to the point of grasping the art of writing academically. To you Nomdayi ndithi ungadinwa nakwabanye, I thank God for your impartation you made in my life.
- To my wife Nomfuneko Victoria “Nhuza” Moni, you were so patient with me when people advised me to desert my studies and I almost gave up. You constantly whispered in my ear that this is possible, thank you love, Ngcolosi, Tiyeka, Mabombo.
- To my kids Libongiwe and Sibabalwe Moni, this is for you guys to take where I left off. This is part of your double portion that is awaiting for both of you. Your future must pass this mile stone.
- The Abha Apostolic Church, for your constant prayers and encouragements when the demons were attacking my God given abilities. You allowed me to stand on your prayers.
- Last but not least to my mother Novotile Nonstikelelo Moni, who always wanted to see her children furthering their studies from young ages. This is for you mamBamba, Thangana, Rhaso, Bodlinja, Krila.

Table of Contents

DECLARATION

ABSTRACT

ACKNOWLEDGEMENTS

LIST OF FIGURES

LIST OF TABLES

GLOSSARY

CHAPTER ONE: INTRODUCTION.....	1
1.1 ALUMINIUM MATERIAL.....	1
1.2 FRICTION STIR WELDING	2
1.3 PRINCIPLE OF OPERATION	2
1.4 BENEFITS OF FSW COMPARED TO FUSION WELDING.....	4
1.5 PROBLEM STATEMENT.....	4
1.6 RESEARCH BACKGROUND	5
1.7 RESEARCH OBJECTIVES.....	6
1.8 THESIS OUTLINE	7
2 CHAPTER TWO: LITERATURE REVIEW.....	8
2.1 INTRODUCTION	8
2.2 TOOL PARAMETERS AND GEOMETRIES FOR 5XXX SERIES ALUMINIUM ALLOYS	8
2.3 FSW ON SIMILAR ALUMINIUM ALLOYS.....	9
2.4 FSW OF 6XXX	12
2.5 FSW ON DISSIMILAR ALUMINIUM ALLOYS	15
2.6 FATIGUE TESTS.....	20
2.7 FRACTOGRAPHY BY SCANNING ELECTRON MICROSCOPY (SEM) ON DISSIMILAR ALLOYS	21
2.8 CLASSIFICATION OF FSW FOR DISSIMILAR ALUMINIUM ALLOYS	24
2.9 EFFECT OF SPECIMEN LOCATION ON THE WELDED PLATES.....	26
2.10 SUMMARY	27
3 CHAPTER THREE: EXPERIMENT SETUP.....	28
3.1 INTRODUCTION	28
3.2 WELDING SET-UP.....	28
3.3 MILLING MACHINE	28
3.4 WELDING PERFORMANCE	29
3.5 SAMPLE PREPARATION	31
3.6 SPECIMEN PREPARATION	33
3.7 EQUIPMENT USED FOR TESTS.....	36
3.8 PERFORMANCE OF TESTS	39
4 CHAPTER FOUR: RESULTS AND DISCUSSIONS.....	45
4.1 FRICTION STIR WELDED JOINTS CHEMICAL COMPOSITIONS.....	45
4.2 METALLOGRAPHIC ANALYSIS.....	47
4.3 MICROSTRUCTURE ANALYSIS	49
4.4 MICRO HARDNESS ANALYSIS	50
4.5 TENSILE TEST RESULTS OF PARENT MATERIALS AND FS WELDED JOINTS.....	55
4.6 BENDING TEST RESULTS OF PARENT MATERIALS AND FS WELDED JOINTS.....	58
4.7 SCANNING ELECTRON MICROSCOPE ANALYSIS	64
4.8 SUMMARY	65
5 CHAPTER FIVE: CONCLUSION AND FUTURE WORK.....	66

5.1	CONCLUSIONS	66
5.2	FUTURE RESEARCH.....	67
6	REFERENCES	68

List of Figures

FIGURE 1.1: PRINCIPLE OF FSW OPERATION (BABU ET AL., 2008)	3
FIGURE 1.2: HULL STRUCTURE MADE OF AA5083 MARINE ALUMINIUM [KUMAR ET AL., 2015]	6
FIGURE 1.3: FSW DECK PANELS FOR CRUISE SHIP [GORDON, 2010]	6
FIGURE 3.1: TRUECUT MECHANICAL SHEARING MACHINE QH11D-3.5 x1250	28
FIGURE 3.2: LAGUN FU. 1-LA MILLING MACHINE	29
FIGURE 3.3: PREPARED PLATES FOR FSW	29
FIGURE 3.4: WELDING SETUP	30
FIGURE 3.5: TOOL GEOMETRY (ALL DIMENSIONS ARE IN MILLIMETRES).....	30
FIGURE 3.6: (A) INSIDE SPOOL AND SPECIMEN TABLE, (B)EDM ACCUTEX AU-500iA WIRE-CUT AND (C) HIDDEN SPOOL AND BRASS WIRE	31
FIGURE 3.7: STRUERS LABOPRESS-3 HOT MOUNTING PRESS	32
FIGURE 3.8: STRUERS LABOPOL 5 POLISHING MACHINE	32
FIGURE 3.9: SAMPLE POSITIONING.....	33
FIGURE 3.10: CAD DRAWINGS FOR TENSILE TEST SPECIMENS (DIMENSIONS ARE IN MM)	33
FIGURE 3.11: CAD DRAWING FOR METALLOGRAPHY AND MICRO-HARDNESS SPECIMENS.....	34
FIGURE 3.12: CAD DRAWINGS FOR BENDING TEST SPECIMENS	35
FIGURE 3.13: SPECIMENS AFTER MOUNTING	35
FIGURE 3.14: ETCHED SPECIMENS.....	36
FIGURE 3.15: HOUNSFIELD TINIUS OLSEN H50KS MACHINE	37
FIGURE 3.16: LIQUID PENETRANT TEST KIT.....	38
FIGURE 3.17: METALLURGICAL INVERTED AE2000 MET MICROSCOPE	38
FIGURE 3.18: VICKERS MICROHARDNESS TESTER (SOURCE: KAMM & VOORT, 1939)	39
FIGURE 3.19: SAMPLING OF SEM SPECIMENS	39
FIGURE 3.20: TENSILE TEST SET-UP ON HOUNSFIELD TINIUS OLSEN H50KS	40
FIGURE 3.21: SPECIMENS FOR TENSILE TESTING	40
FIGURE 3.22: BENDING TEST SET-UP ON HOUNSFIELD TINIUS OLSEN H50KS	41
FIGURE 3.23: BENDING SPECIMENS OF WELDED JOINTS	41
FIGURE 3.24 (A-C): LIQUID PENETRANT APPLIED ON FACE WELD JOINTS	42
FIGURE 3.25: HARDNESS TRAVERSE PROFILE OF CROSS SECTION	43
FIGURE 3.26: MACROSTRUCTURE SET-UP ON HOUNSFIELD TINIUS OLSEN H50KS.....	44
FIGURE 3.27: SPECIMENS READY FOR LOADING INTO SEM	44
FIGURE 4.1: FRICTION STIR WELDED PLATES.....	46
FIGURE 4.2: POST WELD MACROSTRUCTURE.....	47
FIGURE 4.3: MACRO STRUCTURE IMAGES (A-C) 5083 ON AS AND (D-F) 6082 ON AS	48
FIGURE 4.4: PARENT MATERIAL MICROSTRUCTURES	49
FIGURE 4.5: STIR ZONES OF THREE SAMPLES FOR EACH SCENARIO	50
FIGURE 4.6: GRAIN SIZE PATTERN FOR DIFFERENT CONDITIONS.....	50
FIGURE 4.7: MICROHARDNESS PROFILES FOR R5S6, R5M6 AND R5E6 OF RETREATING AA5083-H321	52
FIGURE 4.8: MICROHARDNESS PROFILES ON DIFFERENT POSITIONS WITH AA5083-H321 ON AS	54
FIGURE 4.9(A-B): VISUAL EXAMINATIONS OF TWO SETS 5XXX ADVANCING WHILE 6XXX RETREATING AND VISE VERSA.	55
FIGURE 4.10 (A-B): TENSILE TEST GRAPHS FOR PARENT MATERIALS AND AL-ALLOYS WELDED JOINTS	57
FIGURE 4.11: PARENT MATERIALS BENT JOINTS.....	58
FIGURE 4.12: BENT DISSIMILAR WELDED JOINTS	59
FIGURE 4.13: GRAGHICAL PRESENTATION OF PARENT AND WELDED JOINT MATERIALS.....	63
FIGURE 4.14: SURFACES AFTER LIQUID PENETRANT SOLUTION	63
FIGURE 4.15: SEM MACROGRAPHS.....	64

List of Tables

TABLE 1.1: CHEMICAL COMPOSITION OF 5083-H321 AND 6082-T651[SHANMUGA SUNDARAM & MURUGAN, 2010]	1
TABLE 3.1: FRICTION STIR WELDING PARAMETERS.....	31
TABLE 3.2: ALTERNATIVE POLISHING STEPS USED FOR AL-ALLOYS.....	36
TABLE 4.1: CHEMICAL COMPOSITION OF PARENT MATERIALS AND WELDED JOINTS.....	45
TABLE 4.2: TRAVERSE TENSILE PROPERTIES OF FSW JOINTS	55
TABLE 4.3: ANALYSIS OF THE WELDED JOINTS	59

Glossary

Gas Metal Arc Welding (GMAW) - GMAW is a welding process in which an electric arc forms between a consumable wire electrode and the work-piece metal(s), which heats the work-piece metal(s), causing them to melt and join.

Gas Tungsten Arc Gas Welding (GTAW) - GTAW is an arc welding process that uses a non-consumable tungsten electrode to produce the weld.

Friction Stir Welding (FSW) - FSW is a solid-state joining process that uses a non-consumable tool to join two facing work-pieces without melting the work-piece material. Heat is generated by friction between the rotating tool and the work-piece material, which leads to a softened region near the FSW tool.

Metal Inert Gas (MIG) – MIG is a semi-automatic or automatic arc welding process in which a continuous and consumable wire electrode and a shielding gas are fed through a welding gun.

Tungsten Inert Gas (TIG) - TIG is a welding that utilizes a constant current welding power supply to generate an electric arc between the tungsten electrode and the work-piece, using the resultant heat to create the weld.

Manual Metal Arc (MMA) - MMA is a welding process that uses a consumable electrode covered with a flux to lay the weld.

Coefficient of Friction(COF).

Friction stir processing (FSP) - use of the friction stir process to modify the microstructure to local region metallurgically.

Tool shoulder (TS) - the region of tool in contact with the workpiece surface.

Tool pin (TP) - also referred to as probe or the pin of the tool.

Advancing side (AS) - the tool pin surface rotation direction and the tool traverse direction have the same vectorial sense.

Retreating side (RS) - the tool pin surface rotation direction and the tool traverse direction have the opposite vectorial sense.

Leading edge (LE) - the front side of the tool. The tool shoulder meets the cold

Trailing edge (TE) - the back side of the tool.

Tool rotation rate (TRR) - the rate at which the tool rotates.

Tool traverse speed (TTS) - the travel speed of the tool.

Tilt angle (TA) - the angle between the plane normal of workpiece and the spindle shaft.

Plunge rate (PR) - the rate at which the tool is inserted in the workpiece.

Plunge depth (PD) - the programmed depth of the pin bottom from the top surface of workpiece.

Plunge force (PF) - the vertical force on the tool when shoulder meets the top surface

of workpiece.

Base metal: This is a material that is far from the centre of welding normally found after the shoulders of the tool. This material is not deformed or affected by heat although it may have experienced a thermal cycle from the weld. Its micro -structure or mechanical properties are still intact as they are not affected by the heat.

Heat-affected zone (HAZ): This region is just under the tool shoulder but closer to stirring pin or weld-centre, the material has experienced a thermal cycle that has modified the microstructure and mechanical properties although there is no plastic deformation occurring in this region.

Thermo-mechanically affected zone (TMAZ): TMAZ is found on the edges of the stirring pin where the material plastically deformed as the heat from the FSW process affects the material also. A significant plastic strain without recrystallization in TMAZ is always possible particular in aluminium. It is always clear boundary between the recrystallized zone and the deformed zones of the TMAZ.

Weld nugget (WN): Weld nugget is a transformation of parent material into equiaxed fine-grained recrystallized microstructure formed by plastic deformation and frictional heat generated during FSW. This region is basically along the centre of the mating plates where the centreline of the stirring pin traversed. The fully recrystallized area, sometimes called the stir zone.

Tensile strength (TS), ultimate strength, is the capacity of material or structure to withstand loads tending to elongate/compress the specimen. In other words, tensile strength resists tension, Ultimate tensile strength is measured by the maximum stress that a material can withstand while being stretched or pulled before breaking.

CHAPTER ONE: Introduction

1.1 Aluminium material

Aluminium comes as a pure natural ore which is normally referred to as 1xxx series with a purity of greater than 99.00%. From 1xxx pure aluminium grade, different aluminium alloys are developed through the mixing of different metals to form aluminium alloys. Aluminium materials consists of different grades such as 1xxx - Pure Al, 2xxx - Al-Cu alloys, 3xxx - Al-Mn alloys, 4xxx - Al-Si alloys, 5xxx - Al-Mg alloys, 6xxx - Al-Mg-Si alloys, 7xxx - Al-Zn alloys, 8xxx - Al + other elements, 9xxx - Unused series [Dake, 2018].

When aluminium alloys are formed, the designation is allocated to that alloy to indicate the added alloy. Four-digit number is always used to identify wrought aluminium, where the first digit identifies the main alloying elements, the second single digit if different from 0, indicates a modification of the specific alloy, and the third and fourth digits are arbitrary numbers given to identify a specific alloy in the series.

The designation is then followed by a dash, a letter identifying the type of heat treatment (F - Extruded and air cooled; O - Softened, annealed at 350-500°C, for 1-5 hours; T - Heat treated) and a 1 to 4-digit number identifying the specific temper (T4 - Solution heat treated and naturally aged at 20°C, for 5-10 days, T6 - Solution heat treated, artificially aged, for example). In case of the 5083-H321 and 6082-T651, this will mean that alloy 5083-H321: 5 indicates magnesium, 0 indicates modification, 8 indicates other elements that may be in this alloy and 3 will indicate manganese, while in 6082-T6 alloy: 6 indicates magnesium; 0 indicates modification; 8 indicates other elements that may be in this alloy and 2 will be copper [Davis, 2001].

Table 1.1: Chemical composition of 5083-H321 and 6082-T651 [Shanmuga Sundaram and Murugan, 2010]

Alloy	Si	Fe	Cu	Mn	Mg	Cr
5083-H321	0.40	0.40	0.10	0.40-1.0	4.0-4.9	0.05-0.25
6082-T651	0.7-1.3	0.50	0.10	0.40-1.0	0.6-1.2	0.25

The AA5083-H321 (Al-Mg alloys) are used unprotected for structural and architectural applications. All kinds of welded assemblies such as marine components and tanks always require high efficiency in welding and maximum joint strength. These alloys are used in pressure vessels of up to 65 °C and in many cryogenic applications, bridges, freight cars, marine components, TV towers, drilling rigs, transportation equipment, missile components, and dump truck bodies. Al-Mg alloys are known for good corrosion resistance, easy to weld, moderate to high strength, and not heat treatable. AA5083-H321-Aluminum-Magnesium alloy is characterised by excellent performance in extreme environments. It is resistant to attack by both seawater and industrial chemical environments [Designations et al., 2008].

The 6000 series is an Aluminium-Magnesium-Silicon alloy (Al-Mg-Si alloys). Al-Mg-Si alloys are the most common extrusion alloys and are used particularly in the building industry. AA6082-T651- Al-Mg-Si alloy is characterized by medium strength, good formability, machinability and weldability, corrosion resistant and heat treatable.

Aluminium alloy 6082 is a medium strength alloy with excellent corrosion resistance. Alloy 6082 has the highest strength of the 6000 series alloys. Alloy 6082 is referred to as a structural alloy. 6082 alloy can be used for machining and it also replaced by 6061 alloy in many applications. This alloy is characterised by a large amount of manganese which controls the grain structure that made it to be a stronger alloy. T651 is a solution heat treated, stress relieved by stretching then artificially aged alloy. AA6082-T651 has very good weldability though tends to have a lower strength in the weld zone [El-Shennawy et al., 2017]

Aluminium alloys can be welded using conventional welding methods such as Metal Inert Gas (MIG), Tungsten Inert Gas (TIG), Plasma Arc Welding (PAW), Laser Beam Welding (LBW), Resistance Welding (RW), Electron-Beam Welding (EBW) and Upset Welding (UW). Most of these conventional methods come with range of challenges such as heat input control, hot cracking, porosity and weldable thickness that varies with the process used and that there is no optimal general weld process for all aluminium alloys and thicknesses. While FSW proved to have clamping and tooling challenges but in terms of joint integrity it has been proven to be the best method of welding aluminium alloys [Olabode et al., 2013].

1.2 Friction Stir Welding

Friction stir welding (FSW) is a novel solid-state welding technique of 20th century, invented at The Welding Institute (TWI) in 1991 and was initially applied to aluminium alloys [Givi and Asadi, 2014]. FSW process does not melt the material being welded. FSW process works just below the solidus temperatures of the metals being welded. Friction stir welding is a joining process in which a non-consumable rotating tool plunges into interface of plates which are securely fixed with clamps and fixtures, and after which it moves along the butted surfaces to be welded. FSW uses a rotating tool with a profiled threaded or unthreaded probe whose length is shorter than the weld depth from the tool shoulder.

The FSW process begins by plunging a rotating tool into the interface of the work-piece. Plunging stops when the tool shoulders comes into contact with the surface of the work-pieces. Rotating tool is plunged and dwells for a few seconds and moves along the joint. As the tool traverses heat is generated by the friction action of the tool shoulder against the metal work-pieces.

1.3 Principle of Operation

Hasan et al., (2016) conducted a study on simplified design of clamping system and fixtures for FSW of aluminium alloys. They discovered that sound friction stir welds could be attained by using a proper design of backing/clamping system with a suitable selection of the welding parameters. Parida et al., (2015) adds that the work-pieces are subjected to constant lateral and vertical loads by means of bolts and nuts. Clamping system should be rigid enough to hold the work-pieces securely without unintended gap formation and transverse movement of the work-pieces.

The studies performed under the subject of FSW resulted to the division of FSW into four main stages [Stojic et al., 2016] i.e. Plunging phase, dwelling phase, welding

phase and retraction phase. Each of these phases are described below and shown on figure1.1.

- 1) During the plunging phase, the rotating tool approaches the surface of the metal work-pieces and penetrates into the metal generating the initial heat.
- 2) The dwelling stage includes reaching the working temperature. The temperature is necessary to start the welding until a uniform downward force is reached between the tool and work-pieces. This process continues until the force between the FSW tool and the surface of the metal work-pieces begins to gradually decrease, which indicates that the temperature required to commence welding has been achieved.
- 3) The welding stage includes thermo-mechanical phase. The constant frictional energy generates high temperatures which soften the material at the joining of the plates. Both materials of the work-pieces on the interface are mixed together with the aid of the pin as the tool moves forward in the welding direction.
- 4) The final stage is the retracting stage. The tool is retracted upwards when it reaches the end of the joining line of the work-pieces.

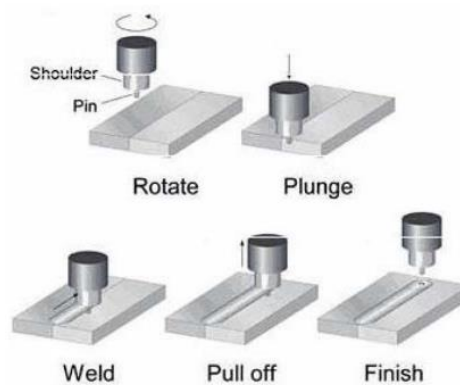


Figure 1.1: Principle of FSW operation [Babu et al., 2008]

The most outstanding feature about FSW is that it operates at the temperature that is below material's melting temperature. The material that is welded through this technique undergoes intense plastic deformation at elevated temperature, resulting in generation of fine and equiaxed recrystallized grains [Mishra et al., 2005]. The fine microstructure in friction stir welds produces good mechanical properties. FSW is considered to be the most significant development in metal joining in a decade and is categorized as a "green" technology due to its energy efficiency, environmental friendliness, and versatility.

FSW uses much less energy. Neither cover gas nor flux is used which makes the process environmentally friendly. As the welding process does not need the use of consumable rods, any aluminium alloy can be joined easily compared to fusion welding. FSW could be applied to different joints such as butt joints, lap joints, T butt joints, and fillet joints [Mishra and Mahoney, 2007].

1.4 Benefits of FSW compared to Fusion Welding

Colligan, (2010) reported that there are technical justifications of FSW over arc welding processes. FSW improves ability of welding different materials together and minimizes post welding metallurgical integrity distortions. FSW has less build-up stress during welding with better fatigue abilities. Joints produced by FSW are known to be resistant to rust and stress corrosion cracking. It improves cosmetic appearance of artefacts and eliminates the under matched filler metal. Friction stir welding improves static strength and ductility of welded joints. Processes in FSW are mechanized processes with high robustness and few process variables needed. FSW does not come without its drawbacks which are outweighed by its benefits, such as: mechanized process, special fixture requirements, joint design limitations and keyhole at end of weld.

FSW is a green and environmentally friendly welding technology because of low energy consumption, no gas emission, and no need for consumable material such as electrodes, no filler metals, and shielding gases (normally present in fusion welding processes) [Kaur et al., 2016]

An experimental investigation on FSW and TIG welding for AA6082 was conducted by Sivaramakrishna, (2015). It was discovered that smooth surface finish can be obtained by using FSW with a tool having a smooth pin. It was further discovered that the microstructure on the heat affected zone (HAZ) was well fused and free from non-metallic defects. In the FSW, the breaking point was outside the welded joint on tensile test whereas in TIG welding the breaking point was exactly on the weld.

Wang et al., (2008) reported the effect of welding processes (FSW and TIG) on the fatigue properties of 5052 aluminium-welded joints. The comparative analysis was performed based on fatigue testing. The results showed that the fatigue properties of FSW welded joints are better than those of TIG welded joints.

A comparative study of conventional fusion welding processes with solid-state welding technique was explored by [Sravanthi, 2016]. The study found that FSW exhibited numerous benefits such as providing opportunities for new solutions to old joining problems, virtually defect-free welding, versatile applications by welding all joint geometries including complex contours, limitless panel length and width, superior mechanical characteristics and join dissimilar alloys.

1.5 Problem statement

Aluminium and its alloys are always difficult to weld using conventional welding processes due to high affinity for each other. Joints for aluminium alloys mainly made of mechanical fasteners which in turn compromise the joint integrity especially in terms of appearance. Various methods are being used in welding aluminium more especially similar alloys. Those methods include TIG, SMAW, GMAW, GTAW and MIEA and the newly discovered one called friction stir welding (FSW) [Ambriz et al., 2018].

This study seeks to demonstrate the weldability of dissimilar aluminium alloys 5083-H321 and 6083-T651 by means of friction stir welding. The two alloys will be friction stir welded with the aid of already converted milling machine and non-consumable tool only. The welding of similar and dissimilar aluminium alloys has been studied since the

discovery of FSW technique. The weld joint for different grades of aluminium alloy behaves differently mechanically. This brings a necessity of studying the behaviour of similar and dissimilar grades when welded through FSW.

1.6 Research background

Metal joining processes are always required in joining of two different materials to take advantage of their mechanical properties in manufacturing industries. These joining techniques are carefully chosen depending on the needs of the assembled component. The welding of Al alloys through conventional fusion welding is difficult to do due to the high temperatures involved particularly with dissimilar alloys [Francis, 2012]. The welding of dissimilar material requires that the material must be compatible with each other in terms of composition. Compatibility must bring different solubility and melting temperatures of the materials together harmoniously.

The introduction of FSW has overcome these material compatibility problems which other joining processes have struggled to overcome. FSW is briefly defined as the new solid state welding process predominantly used in joining the aluminium alloys [Mishra et al., 2014]. This newly evolving technique was developed in 1991 by The Welding Institute based in UK [Thomas et al., 1991]. FSW is beneficial in that being the solid state it eliminates solidification; liquation cracking and porosity which normally evident in other welding processes [DebRoy and Bhadeshia, 2010a]. FSW is mostly associated with grain refinement which in turn improves mechanical properties of the joint [Liu et al., 2018]. FSW works with temperature that is below the melting point of materials and does not require the use of filler rods which can then bring undesirable post problems [Lohwasser and Chen, 2010]. FSW is capable of welding different alloys with ease as long as positioning of the plates is properly done [Thomas and Dolby, 2015].

Pantelis, (2014) defined the FSW of dissimilar metals or dissimilar alloys as the joining of ferrous metals to non-ferrous metal or different alloys that can be used to produce bimetallic components. Such joints can be found in different situations such as automotive, aerospace, and shipbuilding industries, where fusion welding is simply not compatible given the chemical and mechanical incompatibilities between the components to be joined. Generally, this would include problems such as the different deformation behaviour of dissimilar materials, the formation of damaging intermetallic compounds, and differences in physical properties such as thermal conductivity. Assembling of components for aviation, automotive, marine, construction, is compelling all manufacturers to maintain mechanical strength intact and cosmetic appeal after joining components. Due to global warming and environmental awareness campaigns, one needs to factor these in the manufacturing processes [European Aluminium Association, 2015].

Dissimilar blanks of 1 mm thick sheets of AA5182 and AA6016 aluminium alloys were FSWed together as flat sheet of material. The FSW sheets were further processed by a pressing tool to form a deep drawing cylindrical cups. Though the two alloys had different mechanical properties, the FSW joint remained straight and aligned at the middle of the cups after deep drawing [Kumar et al., 2015].

It was reported that Honda Motor Corporation implemented FSW to join dissimilar aluminium alloys and steel in an automobile front structural component in production vehicle Honda Accord. The front sub-frame which carries the engine and the suspension components was made of die cast aluminium and press formed steel halves. Friction stir welding was applied to weld the aluminium to the steel in a lap configuration at various locations. The process of FSW had helped Honda to reduce the body weight by 25%. This weight body reduction translated to approximately 50% reduction of electricity consumption [Yazdipour & Heidarzadeh, 2016].

In Japan, FSW of 5083 (figure 1.2) was used to produce aluminium honeycomb panels and seawater-resistant panels. The panel sizes of 250 mm wide of 5083 aluminium alloy extrusions were FS welded to make panel sizes of 1250 × 5000 mm. The panels were mainly for ship cabin walls and decks because of their good flatness of the weld root.



Figure 1.2: Hull structure made of AA5083 Marine Aluminium [Kumar et al., 2015]

Since 2008 batches of 100t of FSWed AA6082 (figure 1.3) floor panels have been ordered by Marine Aluminium to construct the living quarters for the redevelopment projects in Norway for cruise ship construction.



Figure 1.3: FSW deck panels for cruise ship [Gordon, 2010]

1.7 Research objectives

The aim of this research work is to join 5083-H321 and 6082-T651 aluminium alloys by using the FSW technique. This aim will be achieved through the following objectives:

- Welding of the two dissimilar aluminium alloys
- Comparative microstructural analysis of the joint
- Comparative mechanical properties of the joint
- Fracture analysis of the joint

1.8 Thesis outline

This thesis is composed of five themed chapters.

Chapter 1: Introduction

This chapter deals with problem statement, research background, and outline research objectives.

Chapter 2: Literature Review

This chapter focuses on the literature of Friction Stir Welding. It reviews literature on FSW on similar alloys 5XXX, 6XXX and dissimilar FSW of 5XXX versus 6XXX. These topics are discussed under subsections such as tool parameters and geometries; tensile strengths, bending strength; macrostructures; microstructures and fractographies. It also touches on what has been done, what are the challenges, applications for dissimilar FSW. Finally, it touches on tools as it relates to FSW.

Chapter 3: Experiment Set-up

This chapter describes the overall experimental set-up and methodology. It also outlines topics covered as follows: preparation of material for friction stir welding, friction stir welding process, tensile testing, micro-structure analysis, micro-hardness testing, bending testing, macrostructure, scanning electron microscopy analysis

Chapter 4: Results and discussion

Chapter Four presents the results and discussions of the research welds.

Chapter 5: Conclusion and future work

Chapter Five is the conclusion; this includes a discussion on possible future work and development.

Chapter Two: Literature Review

2.1 Introduction

This chapter explores different aspects of literature as it relates to listed objectives of this study. It uses different case studies to establish feasibility of each aspect. It starts by discussing FSW in general, FSW of similar and dissimilar Al alloys, and effect of extracting specimen location on the joint, delve into mechanical properties and summaries the literature review.

2.2 Tool parameters and geometries for 5XXX series aluminium alloys

Friction stir welding (FSW) is governed by set of process parameters that are set for a particular weld run. These parameters affect joint integrity and quality of the post welding features that cannot be reversed. It is for this reason that these parameters are properly determined beforehand. Parameters that will be discussed under this section are tilt angle, rotational speed, traversing speed and dwell time.

Study on friction stir welding of aluminium alloy 5083-O was performed by [Klobčar et al., (2012)]. The study attempted to verify the weldability of 5083-O to 5083-O by means of FWS. The 4 mm thick plates were joined using a concave shoulder threaded cylindrical pin. The rotational speed and welding speed were varied where 200 rpm was the minimum rotational speed, 1250 rpm was the maximum rotational speed, the lowest welding speed was 71 mm/min and highest welding speed was 450 mm/min. The welded joint exhibited 15% drop of tensile strength compare to base metal with a further drop on hardness observed on the advancing side of the welded joint. The best results were obtained from the combination of 360 mm/min and 1100 rpm

Jesus et al., (2016) performed three tool geometrical analyses on FSW 5083-H111 T-joints. The tool pin profiles used included tapered and threaded, quadrangular pyramidal and progressive pin, part threaded cylindrical and part pyramidal with all concave shoulders. None of the tool pin profiles affected hardness of the welded joint significantly. Progressive pin tool produced best tensile strength equivalent to base metal while pyramidal pin tool delivered tunnel and kissing-bond defects with the presence of oxide line on joints produced by tapered pin tool.

An investigation work aimed at getting the optimum process parameters for 5083 aluminium alloy was performed by [Bayazid et al. 2015]. Plane tool was used at speeds of 1120 rpm and 40 mm/min while triangular tool used 1400 rpm and 63 mm/min speeds. The study discovered that tool rotational speed has less effect on hardness than the tensile strength while weld speed has more effect on the tensile strength and the hardness of the welded joint.

Jaiswal et al., (2014) performed assessment study on AA5083-H111 joint. The objective of the assessment was to explore the relationship between FSW variables such as tool profile, rotating speed, welding speed and the mechanical properties. Tapered smooth, tapered threaded and triflute high speed steel tools (HSS) were used. All the tool rotational speeds were set at 600, 800 and 1000 rpm against constant 50 mm/min. The joint that was produced by means of triflute tool contributed to the best mechanical achieved compared to tapered smooth and threaded tool.

Alali and Injeti, (2016) reviewed numerous studies with the aim of identifying gaps from the available studies of FSW on 5083 aluminium alloy. The focus was on microstructural and mechanical properties. The effect of welding parameters namely welding speed and rotational speed on the mechanical properties and microstructure of the 5083 FS welds was argued. The studies focussed on impact of rotational and welding speeds on mechanical properties. The study proposed more research on other welding parameters on the quality of joints made by FSW effect of rotational and welding speeds on the mechanical properties and microstructure of the welds.

A study on effect of FSP parameters on the mechanical and thermal behaviour of 5754-H111aluminium plates was conducted by Serio et al. (2016). Two plates of 6 mm thickness were joined by means of FSW using rotational speeds of 500 and 700 rpm against traverse speeds of 200 and 300 mm/min. The tool had a shoulder diameter of 22 mm with a pin length of 5.8 mm and a tool tilted at 1.2°. Circular ripples that were attributed to the surface of the tool shoulder were observed on the surface of the welded joints. With speed combination of rotational speed of 500 rpm and traverse speeds of 200 and 300 mm/min, the welded joints had no visual defects while 700 rpm and 300 mm/min had tunnel voids and excessive flashes on the advancing side. Both joints exhibited lateral penetration of the tool as there were no partial welding observed. The study observed that temperatures on the retreating side were higher than the advancing side which caused UTS to increase with temperature.

The optimization of welding parameters is a subject that is in progress. This includes the use of similar aluminium alloys in optimizing some welding parameters. Kundu and Singh, (2016) recently conducted FSW parameter optimization study using aluminium alloy AA5083-H321. The Taguchi's L9 orthogonal array was used for the analysis of the three parameters – tool rotational speeds (500 rpm, 950 rpm and 1400 rpm), traverse speeds (16 mm/min, 28 mm/min and 40 mm/min) and tilt tool angles (1°, 2° and 3°). Tool rotational speeds were kept constant against varied traverse speeds and tool tilt angles. It was discovered that the optimum values of the process parameters for higher UTS and higher micro-hardness were tool rotational speed of 950 r/min, traverse speed of 28 mm/min and tool tilt angle of 3°. It was also found that tool rotational speed and traverse speed were dominating parameters.

2.3 FSW on similar aluminium alloys

Welding of similar alloys is a normal practice in various industries. This section is reviewing the progress towards the use of FSW in joining similar 5xxx aluminium alloys. This review is looking at different aspects that each reported work focused on tool parameters and geometries, tensile tests; bending tests, macrostructures, microstructures and microhardness.

2.3.1 Tool parameters and geometries for 5xxx series aluminium alloys

Friction stir welding (FSW) is governed by set of process parameters that are set for a particular weld run. These parameters affect joint integrity and quality of the post welding features that cannot be reversed. It is for this reason that these parameters are properly determined beforehand. Parameters that will be discussed under this section are tilt angle, rotational speed, traversing speed and dwell time.

An experimental study on effects of FSW parameters on joint properties of AA5754 was embarked upon by [Ozsarac, 2012]. The aim was to evaluate the effects of the tool rotation speed, tool tilt angle, and tool rotation direction on the FSW of AA5754. Rotational speeds of 700, 900 and 1100 rpm together with constant traverse speed of 13 mm/min were used. The tool used was a hot work steel material, known as type 1.2344. The tool had a concave shoulder diameter of 15 mm with a conical threaded pin of 5 mm in diameter. Three batches were FSWed. First batch used 2° tool tilt angle in clockwise direction. Second batch used 0° tool tilt angle in clockwise direction. Third batch used 2° tool tilt angle in anti-clockwise direction. The weld joint of 700 rpm and 2° tool tilt angle in anti-clockwise direction did not weld properly at all. The joint had tunnel and cavity defects which were attributed to the combination of 700 rpm and 13mm/min. The study suggested that this was caused by the metal pushed into the bottom of the plates by the threaded pin. This was also considered as abnormal stirring of the metal with insufficient heat input for mixing properly. Second batch was characterized by a noticeable weld flashes on retreating side. First batch was characterised by basin-shaped nugget zone formation which was broadened for both the advancing side and retreating side closer the upper surface. Although second batch joints were generally similar to the first batch joints, these joints showed a narrower basin-shaped weld stir zone with changing of the tool tilt angle. The stir zones in second batch were noticeable changed with changing of the tool rotation direction. The study observed that the tool tilt angle, tool rotation direction, and tool rotation speeds had an effect on the defect formation and weld penetration depth. The defects were formed underneath the pin for the joint in first and second batches. The cavity defects were only formed on the retreating side for first batch, whereas it was formed on both the retreating and advancing sides in second batch. The study concluded that the surface roughness of the trials improved with the increase of the rotational speeds.

Sangalli et al., (2019) qualified the FSW of AA5083-O and AA5052-O. The study employed speed combinations of 1450 rpm and 20 mm/min. Two different tools were used. The first tool was a tapered triangular threaded pin with a shoulder diameter of 7 mm. The second tool was tapered cylindrical threaded pin with a shoulder diameter of 7mm as well. Eight pairs of plates were FSW together. Firstly, two pairs of AA5083 at retreating with AA5052 at both thickness of 6.35 mm with triangular tool. Secondly, two pairs of AA5083 at retreating side with AA5052 with a thickness of 6.05mm with triangular tool. Thirdly, two pairs of AA5083 at retreating side with AA5052 with a thickness of 6.05mm with cylindrical tool. Fourthly, two pairs AA5052 at retreating side with AA5083 with a thickness of 6.05 mm with cylindrical tool. The study observed that, with welding parameters of the first and second pairs, the tensile specimens broke on the weld interface. An average of ultimate tensile strengths of 156 and 167 MPa for the first and second pairs were recorded. These joints also did not reach bent angle of 150° on face bending during bending testing. Third and fourth pairs obtained similar results in tensile testing. The average ultimate tensile strengths for the third and fourth pairs were 188 and 190 MPa, respectively.

2.3.2 Tensile tests on AA5XXX

Saravanakumar et al., (2018) investigated FSW of AA5083-H32 aluminium alloy by changing the process parameters. Rotational speeds of 710, 900, 1220 and 1400 rpm were used with traverse speed of 20 and 40 mm/min. Circular smooth and circular threaded tool pins were used. Rotational speeds of 710 rpm and 900 rpm were set against feed rate of 20 mm/min while 1220 rpm and 1400 rpm were against 40 mm/min

for both pins. The study concluded that at 1200 rpm at the feed rate of 40mm/min, good weld was achieved. This speed combination achieved micro hardness 86.7 VHN and tensile strength of 205.1 N/mm² in circular threaded tool.

Marhoon et al.,(2018) studied mechanical properties of AA5086 aluminium alloy FS welded joints. Rotational speeds of 1500, 1700 and 1900 rpm were used with a constant welding speed of 60 mm/min. Welded joint of 1700 rpm versus 60 mm/min achieved whopping 84% UTS of the parent material while 1900 rpm and 1500 rpm combinations achieved 79% and 71% respectively. Joint efficiencies correlated with UTS percentages.

A study of effects of FSW on aluminium alloy 5083 was conducted by [Ravindar and Gururaj, 2015]. The aim was to determine the effects of FSW parameters. Parameters that were considered were the tool rotation speed, feed rate, angle of tool tilt. Tool rotational speeds ranged from 700 to 1100 rpm while traverse speeds ranged from 60 to 100 mm/min and tool tilt ranged of 90 to 91°. Study reported that tool rotational speed 1100 rpm, traverse speed of 100 mm/min and tool tilt angle of 91° produced joint with tensile strength of 255.464 N/mm², yield strength of 184.539 N/mm² and percentage elongation of 8.28%. These results were better results when compared to other combinations.

2.3.3 Bending tests on 5xxx

Çam et al., (2009) conducted an investigative study on AA5086-H32. The study looked into the effect of welding speeds of the FS welded joint. Bending, tensile, micro-hardness and microstructure were measured. The constant rotational speed of 1600rpm was used with changing traverse speeds of 175, 200 and 225 mm/min. The joint produced with the speed combination of 1600 rpm and 175 mm/min was characterized by insufficient penetration of the tool which caused kissing-bond defects resulted in low bending strength of the welded joints. The joints produced with 1600 rpm and 200 mm/min and 1600 rpm and 225 mm/min managed to achieve 75% and 74% of the bending strength respectively. The study also observed that bending tests were in agreement with tensile tests that they both show congruent pattern of graphs.

Nur et al., (2017) analysed bending strength of friction stir welded aluminium alloy 5052. The study explored the effect of shoulder diameter sizes where 17.8 and 25 mm shoulder diameter were used. Both tool pins had similar smooth cylindrical tapered geometries. Rotational speeds of 855, 1300 and 1950rpm were set against feed rates of 50, 135, and 208 mm/min. The highest results for face and root bends were produced by combination speed of 1300 rpm and 208 mm/min both in 17.8 mm shoulder diameter which achieved 107% and 110% of flexural bending strength respectively. The least strength for face bend was found in shoulder diameter 17.8 mm with combination speeds of 1950 rpm and 208 mm/min to be 4.76% while for root bends at 1300 rpm and 208 mm/min speeds in 25 mm shoulder diameter achieved 5.26%.

2.3.4 Macrostructures, microstructures and microhardness on AA5XXX

A characterisation study on mechanical and microstructural of friction stir welded 5083 aluminium alloy was conducted by [Shiva Chander et al., 2018]. A 4 mm thick plate of 5083 was FS welded at a constant traverse speed of 40 mm/min and 900, 1120, 1400 and 1800 rpm. Taper threaded and conical taper profile tools were used. The maximum

microhardness value was achieved at 1800 rpm while the minimum was achieved at 1400 rpm for conical taper tool. The threaded taper tool profile had a maximum microhardness at 900 rpm while its minimum was achieved at 1800 rpm. The small size grains were observed at tool rotation speed of 1400 rpm with conical taper tool. The entire weld was characterized by small sized grains across the welded joint as a results of recrystallization. The thermo-mechanical affected zone had a slightly elongated grain structure attributed to the annealing effect of heat and rigorous plastic deformation of material around the pin circumference. In the TMAZ, the material was plastically deformed by using conical taper tool profile. The TMAZ produced by taper threaded tool was not deformed plastically at 1120 rpm.

Vilaça et al., (2006) conducted a study on metallurgical and corrosion features of FSW of AA5083-H11. A 4 mm thick plate of AA5083-H11 was friction stir welded at a rotational speed of 1120 rpm and the traverse speed was 320 mm/min. Two different tools were used. Firstly, a 15 mm shoulder tool, smooth concave with 7° and M5 cylindrical threaded pin with 3 flats of a 3.9 mm length which was operated at 2° tilt angle. Second tool had 17 mm shoulder, flat with 3 concentric striates of 2mm depth with 3.9 mm length tilted at an angle of 1°. Results showed that the different shoulder geometries did influence the surface finishing. With the first tool, the grains in the thermo-affected zone and heat affected zones had maintained same sizes. The grains had an increased deformation closer to the interface with the stir zones. With the second tool, thermo-mechanical affected zones and stir zones interface enhanced the significant difference between the structure of initial grain and the grain resultant of the dynamical recrystallization process defining the stir zone. Hardness values showed an increase towards the welded joints from parent materials. First tool recorded highest hardness values (84 HV1) on the HAZ of the advancing side. The second tool recorder its highest hardness value of 82 HV1 on the retreating side.

2.4 FSW of 6XXX

Welding of similar alloys is a normal practice in various industries. This section is reviewing the progress towards the use of FSW in joining similar 6XXX aluminium alloys. This review is looking at different aspects that each work reported focused on tool parameters and geometries, tensile tests; bending tests, macrostructures, microstructures and microhardness.

2.4.1 Tool parameters and geometries on 6XXX

The impact of welding parameters variation on the properties of FSWed AA6082-T6 joints was investigated by [Adamowski and Szkodo 2007]. Tool rotational speed used ranged from 230 rpm to 1700 rpm against a traverse speed ranged from 115 mm/min to 585 mm/min with a cylindrical threaded tool. It was observed that all specimens failed in heat affected zone of the advancing side. It was also observed that tensile strengths of FSW welded joints were directly proportional to the weld speeds. A nugget zone exhibited a drop in hardness which correlated with heat affected zone on advancing side where tensile tests failure occurred.

Tool design influence on mechanical properties in FSW of AA6082-T6 was investigated by [Ramesh and Rani, 2016]. Uniform tool rotation speed of 900 rpm and welding speed of 40 mm/min were used. Tool pin geometries were varied as square pin, threaded tapered screw pin and threaded straight cylindrical pin. Results established that the shape of the pin has a significant effect on the joint integrity and the mechanical properties. Square pin produced 85% joint efficiency to that of base metal.

While joining dissimilar alloys is flourishing in metal industry, geometric consideration of tools has proven to be critical. Ranjith and Kumar, (2014) have performed the FSW of dissimilar aluminium alloys (AA2014 T651 and AA6063 T651) with the purpose of optimizing the welding parameters. The weld was obtained by varying tool tilt angle between (2° - 4°), tool offset (0.5 mm towards AS, centre line, 0.5mm towards RS) and pin diameter (5 mm – 7 mm). It was observed that at 4° tilt angle optimum interlocking and bonding of materials was achieved while tensile strength was superior when the tool was offset towards AA2014-T651 side. This was attributed to complete fusion of harder material. When offset was towards AA6063-T651 side resulted in poorer heat was generated on advancing side. Heat generation was produced mainly by pin diameter. Pin diameter when it was offset towards the advancing side at 4° tilt angle achieved tensile strength of 87.7% strength of the base metal. It was discovered that the best tensile strength was attained when the pin diameter is equal to the thickness of the plate.

2.4.2 Tensile tests on 6XXX

Valate et al., (2016) investigated variation in tensile strength of FS welded joints of 6mm thick AA6082-T6 aluminium alloy. The objective was to ascertain the effects of varied welding speeds, rotational speeds and tool pin geometries on the quality of welded joints. Cylindrical smooth taper and cylindrical screw thread tool pins were used. Tool pins had comparative dimensions of 4 mm, 12 mm diameter and shoulder diameters respectively except that the length of cylindrical smooth taper was 0.4 mm shorter than that of its competitor. Combination speeds employed ranged from 800, 1000 and 1200 rpm with 30, 60 and 80 mm/min. Tensile strength of 60% to that of the parent material was achieved with cylindrical threaded geometry on the speeds combination of 30 mm/min and 1200 rpm while the cylindrical smooth taper tool pin achieved only 48% tensile strength of the parent material at 1000 rpm and 60 mm/min.

Tensile tests, as part of mechanical properties were conducted in 6063 aluminium by [Sashank et al., 2018]. The objective was to understand the effects of rotational speed and welding speed in the range of 700 – 1500 rpm and 60 – 100 mm/min, respectively. FSW was achieved using high speed steel tool with shoulder diameter of 15 mm, pin diameter of 4 mm, cylindrical pin length of 2.7 mm on a 3 mm thick plate. A combination tool rotational speed of 700 rpm and welding speed of 60 mm/min produced best tensile strength and ductility when compared to other combinations. This combination achieved 80% of base material tensile strength while other combinations achieved far less.

Babu et al., (2008) conducted experimental study on aluminium alloy 6082. The aim was to evaluate the effects of welding speeds on mechanical properties with tensile

testing included. A plate of 5 mm thickness was used. What was also of interest was the use of high speed steel (HSS) tool with 20 mm shoulder diameter with 5mm diameter pin and a length of 4.9 mm. Rotational speed and welding speed in the range of 460 – 1700 rpm and 115 – 585 mm/min, respectively. All specimens failed at heat affected zone on the advancing sides. It was observed that with rotational speeds kept constant, the ultimate tensile strength and tensile strength were direct proportional to welding speeds.

2.4.3 Bending tests on 6XXX

Srinivasulu et al., (2015) evaluated bending strength of FS welded 5mm thick plate of AA6082 aluminium alloy. A taper cylindrical tool pin profile with shoulder to pin diameter ratio of 3 at 0° tool tilt was used. The study used combination speeds of 1800 rpm versus 30 and 50 mm/min and 2400 rpm versus 30 and 50 mm/min. Parent material achieved 180° bend while the all the fabricated joints broke far less than 90°. It was observed that both face and root specimens in all speeds combinations were failing at the HAZ of the advancing side of AA6082 which also exhibited low hardness values. Combination of 2400 rpm and 30 mm/min showed better results than other combinations. Face bends performed better than root bends. It was observed that root bends were characterized by tunnel defects. More defects were found in the joints fabricated at a rotational speed of 1800 rpm and welding speed of 50 mm/min.

Joint properties of FSWed 6 mm thick plates AA6061 alloy were evaluated by [Chandru et al., 2017]. Tool rotational speeds of 700, 800 and 900 rpm and the welding speeds of 22, 30 and 40 mm/min were used. A smooth tool pin of 7 mm diameter, 25 mm shoulder diameter and a pin length of 5.8 was used. Traverse speed of 40 mm/min with rotational speeds of 700, 800 and 900 rpm performed well. These combinations also recorded the highest bending strength ranging from 733 to 1000 MPa. The highest bending strength of 1000 MPa was obtained at 800 rpm and 40 mm/min.

2.4.4 Macrostructures, microstructures and microhardness on 6XXX

Krzysztof and Kurtyka, (2015) carried a study on microstructure and properties of FSWed AA6082 with different welding parameters. A 6 mm thick plate was friction stir welded at 710 rpm versus 710 mm/min. The conventional threaded 8 mm diameter tool pin and a spiral grooved shoulder diameter of 25 mm in 1.5° tilt angle were used. Joints were friction stir welded parallel to the rolling direction of the material. Samples were investigated two weeks after being friction stir welded to allow natural ageing. Defects were observed at the combination speed of 710 mm / min 710 rpm. On the advancing side of the welded joint, the microstructure exhibited different severe border of fine microstructure while retreating side had a homogeneous microstructure. Fracture specimens from scanning electron microscope (SEM) were characterised with less bonded surfaces which gave rise to the lower strength of the weld area. Micro hardness distribution near the weld face was diminished across the width of the tool shoulder.

An investigative study to understand the microstructure and mechanical properties of FSW 6063 aluminium alloy was conducted by [Sashank et al. 2018]. Speed

combinations of rotational speeds of 700, 1000 and 1500 rpm and traverse speeds of 60 and 100 mm/min were used under constant 3° tilt angle. A cylindrical tool of 15mm shoulder diameter, 4 mm pin diameter with a pin length of 2.7 mm was used on a 3 mm thick plates. Generally, deformity and elongation of grains with different sizes and stir zone had equiaxed grains. The average grain size of the parent material measured about 3.3 - 4.6 μm . TMAZ and HAZ and were partly recrystallized and characterized by less uniformly grain sizes compared to stir zone. Welding joint produced with 1500 rpm and 60 mm/min had severe macro structural defects while speed combination of 700 rpm and 60 mm/min had defect free joint. Traverse hardness pattern followed “W” pattern as was found by [Moreira et al., 2009]. It was observed that hardness increased with the decreasing tool rotational speed which attributed to the refinement of grain size. Advancing side was characterized by the lowest hardness in the stir zone because of the relatively higher heat input.

2.5 FSW on dissimilar aluminium alloys

This section is reviewing the progress made towards the use of FSW in joining dissimilar aluminium alloys. This section reported on tool parameters and geometries, tensile tests; bending tests, macrostructures, microstructures, micro-hardness, scanning electron microscope and fatigue. Dissimilar alloys refer to joining materials that are different in mechanical properties, chemical composition, thermal properties or structure.

An review study into some of the friction stir welding work performed was conducted by [Soeripto, 1998]. The study made a review of different works into the importance of FSW. It was discovered that replacement of fastened joints with FS welded joints can lead to significant weight and cost savings, reliably alternative for many industries.

Śliwa et al., (2019) conducted an investigative study on possibilities of joining different metallic parts of structure using FSW methods. The study performed an experiment of joining 2024-T3 and 5182 alloys. The joints were joined by means tungsten carbide tool. The tool rotational speed ranged from 1500 to 3000 rpm, traverse speed ranged from 50-100 mm/min with a dwell time of 20 sec. The possibility of joining 2024-T3 and 5182 was achieved. The study observed that the transportation industry, particularly the automotive and aviation sectors, has strongly committed to reducing the mass of the construction. It was further noted that the process of reducing weight of a vehicle/aircraft is mainly conducted by replacing steel components by lightweight materials such as aluminium alloys.

2.5.1 Tool parameters and geometries on dissimilar alloys

FSW of dissimilar alloys AA6082-T6/AA5083-O was investigated by [Jain et al., 2017]. The aim was to study the influence of different FSW parameters using Taguchi, grey relational and weight method. Four welding parameters were investigated, namely tool rotation speed, welding speed, tool pin profile and shoulder diameter. Only three parameters, i.e. tool rotation speed, welding speed and shoulder diameter that mainly affect the UTS and tool pin profile played a non-significant role for evaluating UTS. For UTS, tool rotation speed emerged as the most significant with a contribution of 64.08%, followed by welding speed (29.55%); tool shoulder diameter (5.67%). While for

elongation, tool rotation speed had also further emerged as the most significant with 48.29%, contribution followed by welding speed (11.06%); tool shoulder diameter (36.71%).

This agrees with Kundu and Singh, (2016) where they conducted a similar study and concluded that tool rotation speed, tool shoulder and welding speed were dominating parameters for FSW and have influence on UTS.

An experimental study on similar and dissimilar FSW of aluminium alloys (5083-H111 and 6082-T6) was conducted by [Kumar et al., 2018]. This study was performed to investigate the mechanical properties on a 6082-T6 aluminium alloy. Constant tool rotational speed 1200 rpm, tool tilt angle 1° and welding speed 63 mm/min were used. The study concluded that efficiency of the welded joint, hardness of dissimilar alloys tested were superior to similar aluminium alloys. The morphology of the joint showed good fusion of intermetallic compounds without any defects. It was also discovered that it is preferred to clamp the higher tensile strength material (5083-H111) towards retreating side and lower tensile strength material towards advancing side (6082-T6) to acquire superior tensile properties.

2.5.2 Tensile tests on dissimilar alloys

A study of FS welded dissimilar AA6061-T651 and AA7075-T651 alloys with different process parameters such as tool rotation, welding speed and tool pin profiles were conducted by [Sathari et al., 2015]. The focus was on effects of the tool rotational and welding speeds towards the tensile strength of the joint. The pin profiles versus micro hardness distribution and tensile property of the joints were also studied on condition that AA6061-T651 plate was on the advancing side. The study showed that the tensile strength was better when AA6061-T651 was placed on the advancing side. Fracture occurred on the heat-affected zone on the AA6061-T651 side during tensile testing, where micro hardness value is less. Lower welding and higher rotational speed produced good mixing of the joined materials. The study concluded that in dissimilar friction stir welding, the weaker materials should be placed on the advancing side to activate the heat from the tool rotation to smoothen the material flow formation in the stirred zone.

Navaneethakrishnan and Ganesh, (2015) investigated the effect of welding parameters on FSW dissimilar aluminium alloys 7075-T6 and 6082-T6 with various tool pin profiles. Cylindrical, square and triangular profile pins were used. All the tools were made of H13 high speed steel. Tool rotational speed of 1250 rpm and traverse speed of 50 mm were used for all the different tools. Report showed that cylindrical threaded tool pin performed better than the triangular pin geometrical when comparing the tensile strength and ultimate strength of the joints. The microstructure for cylindrical tool had a good flow of alloy and fragmented particles.

Palanivel et al., (2014) evaluated mechanical and metallurgical properties of dissimilar friction stir welded on 6 mm thick AA5083-H111 and AA6351-T6 aluminium alloys. A high carbon and high chromium steel (HCHCr) with straight square (SS) pin profile was used. The tool with tool shoulder diameter of 18 mm, pin diameter of 6 mm and pin length of 5.7 mm was employed. Traverse speeds of 36, 63 and 90 mm/min were used to friction stir weld the joints. The tool rotational speed was uniform at 950 rpm. The

ultimate tensile strength was found to be the highest at a traverse speed of 63 mm/min, followed by traverse speeds of 90 mm/min and 36 mm/min respectively. Joints produced by 36 and 90 mm/min had defects which gave rise to joint weakening. Joints at 36 and 63 mm/min specimens broke at the centre while specimen produced by 90mm/min broke at AA6351 side. The ductile fracture was observed on the joint produced by 63 mm/min.

2.5.3 Bending tests on dissimilar alloys

Gungor et al., (2014), evaluated mechanical and microstructural properties of friction stir welded 5083-H111 and 6082-T651 aluminium alloys. Welding parameters of tool rotating speed of 1250 rpm, traverse speed of 64 mm/min and tool tilt angle of 2° were used. The H13 tool steel was employed in the study. Similar joints of 5083-H111–5083-H111 and 6082-T651-6082-T651 and dissimilar joints of 5083-H111 –6082-T651 aluminium alloys were fabricated with these parameters. It was found that similar alloys 5083-H111 achieved average bending strength of 86% of the based metal bending strength. Dissimilar welding of 5083-H111 and 6082-T651 achieved bending strength of 65% while similar FS welding of 6082 achieved 62% bending strength.

A study on mechanical properties of FSW joints on 6mm thick similar and dissimilar AA6061 & AA6082 was conducted by [Naimuddin, 2016]. Non-destructive test and bending tests were conducted. Three pairs of friction stir welded joints were produced. Firstly, similar alloys of AA6061 & AA6061 was produced at speeds of 900 rpm and 50mm/min. Secondly, AA6061 & AA6082 was produced at 1120 rpm and 50 mm/min and lastly AA6082 & AA6082 was produced at 1400 rpm and 50 mm/min. The tool employed was having a tool shoulder of 18 mm, 6 mm tool pin diameter with a tool length of 4.7 mm. A speed of 1 mm/min was used during bending tests to achieve an angle of 180° bend for all joints for the joints. All the joints achieved 180° bend but different bending strength were observed. A similar alloys AA6082 to AA6082 achieved 2.130 kN at 180° bend, dissimilar alloys AA6061 to AA6082 achieved 1.79kN at 180° bend while AA6061 to AA6061 achieved load of 1.730kN at 180° bend. It was noted that at 180° bend, dissimilar alloys AA6061 to AA6082 had a deflection of 30 mm, similar alloys AA6061/AA6061 and AA6082/AA6082 achieved 20 and 24 mm deflections respectively. Liquid penetrant test was applied before bending tests to check cracks and voids on the welded joints. Results revealed a non-defect surfaces of the welded joints. No root flaws or other defects were detected in all joints.

Das and Toppo (2018) performed three-point bending analysis on the joints formed through FSW of AA6101-T6 and AA6351-T6. A high carbon high chromium steel taper cylindrical threaded tool pin was used. It had shoulder diameter of 25 mm and a tapered pin with diameter going from 8 mm and 11.7 mm in length. Three rotational speeds of 900, 1100 and 1300 rpm of the tool with a uniform traverse speed of 16 mm/min were utilized. Bending test was done on a crosshead speed of 0.5 mm/min to avoid the over straining of specimens. Friction stir welded joints of AA6101 produced by 1100 rpm and 16 mm/min speeds achieved an enormous 138% of AA6101 flexural strength. The joints produced by 1300 rpm and 16 mm/min and 900 rpm 16 mm\min achieved 94 and 93% of flexural strength of AA6101 respectively.

Three-point bending tests were done on the 5 mm thick FS welded joints of AA6082 and AA7075 by [Kasman, 2013]. Plates were FS welded using two 18 mm shoulder diameter tools of straight smooth tool pins and cylindrical threaded pin of 5 mm. The other two were 20 mm shoulder diameter with straight smooth pin and cylindrical pin of 6mm diameter. The speed that were used are 500, 630, 800 and 1000 rpm and 40, 63, 80 and 100 mm/min. Sixteen sets of joints were processed from these tool rotational and traverse speeds. All the FSW joints managed to reach a 90° bend with no defects observed except for rotational speed of 1000 rpm combined with 40, 63, 80 and 100 mm/min in 18 mm diameter cylindrical tool. The cylindrical threaded tool at 800 rpm and 63 mm/min of 20 mm shoulder diameter and 6 mm tool pin also had defects and could not reach 90° bend. Crack happened on the heat affected zones of AA6082-T651. It was also observed that bending occurred at the side of AA6082 and no cracks were observed.

2.5.4 Macrostructures, microstructures and microhardness on dissimilar aluminium alloys

This section reviews the work done on microstructures, macrostructures and microhardness for AA5XXX series and AA6XXX series.

Three microstructural weld joint zones of FSW, that is heat affected zone, thermo-mechanical affected zone and weld nugget were reported by Patel et al., (2019) in FSW of AA5083-AA2024. The formation of different zones was a result of thermal and mechanical deformation that the tool at a certain speed induced during welding. Weld nugget was transformed drastically into fine grain microstructure as part of grain refinement, whereas the thermo-mechanical affected zone had an elongated grain structures. Hardness values were found to be the lowest in the heat affected zone as a results of coarseness of the grain particles in the heat affected zone.

A case study of friction stir welded of dissimilar 6082 and 5083 aluminium alloys was conducted by [Kasman et al., 2013]. The study used two different tools to friction stir the weld the joint. The tools used had pentagonal and triangular shaped pins. Both tools had shoulder diameters of 20 mm and operated at 2° tilt angles. Tool rotational speeds were 400, 500, 630 and 800 rpm together with traverse speeds of 40, 50 63 and 80 mm/min. The prominence of onion rings in the stir zones produced by a pentagonal-shaped pin was more distinctive and the width of stir zones were higher compared to the triangular-shaped pin. The shapes of the onion rings were also similar for the entire weld joints and characterized by an elliptical pattern. The small populated defects at the root of weld joint were noted on both the advancing and retracting side. The population of defects was attributed insufficient heat input. A triangular shaped pin at 800 rpm and 80 mm/min produced best welding joint as there were no defects found. The triangular shaped pin at 800 rpm and 80 mm/min speed combination also showed highest values in UTS and joint efficiency.

A study of FSW of similar and dissimilar AA5083 and AA6061 for automotive applications were conducted by [Selamat et al., 2016]. Combination speed of 1000 rpm and 100 mm/min was used. H13 threaded tool pin of 4.7 mm length and diameter of 5mm was used at tilt angle of 3°. Three pairs of FSW joints of AA5083/AA5083, AA6061/AA6061 and dissimilar AA5083/AA6061 were made. During dissimilar welding AA5083 was placed on advancing side. Macrostructures of AA5083/AA5083 showed

no defect on the welded joint. The microstructures were characterized by stir zone, heat affected zone, and thermo-mechanical heat affected zone. Distinctive onion ring patterns were observed on the friction stir welded joint of AA5083-AA5083. Different patterns and grain sizes of the stir zone in the welded joint were produced. Patterns were ascribed to the parameters used during the FSW process particularly the rotational tool and traverse speeds. Recrystallization occurred during the FSW process as the fine grain size in the stir zone was observed. For similar alloys, micro-hardness values were uniform across the weld joint while dissimilar alloys showed a drop in micro-hardness values were observed on the AA6061 side. In contrasting results, the study of joining of AA5083 and AA6061 by FSW conducted by [Shigematsu et al., 2003] found an increased in micro-hardness values on AA6061 side. During etching, the macrostructure of the welded joint of the dissimilar alloys were characterised by contrasting colours due to different reactions to chemical reagent after being etched. AA5083 appeared darker compared to AA6061.

Kumar et al., (2014) conducted a study of optimizing the process parameters of FSW between AA5083 and AA6082. Tool rotational speeds of 710, 1000 and 1400 rpm and uniform traverse speed of 20 mm/min were employed. Circular and square tool pins were used. In the weld nugget the onion ring pattern was observed in a lamellar arrangement. Grains parent materials were noted to be non-equiaxed with grain sizes. The grain sizes were in parent materials were bigger than 100 μm while the nugget were characterized by smaller equiaxed grains. Grain sizes were noted to be direct proportional to tool rotational speeds irrespective of the tool pin profiles. Also grain sizes in the thermal affected zone were bigger than in the stir zone. A hardness values decreased across the thermal affected zones. AA6082 had lower hardness in the stir zone than that of AA5083. The hardness was not affected by the change of the tool pin profile while the increase in tool rotational speed resulted in decreased hardness values.

Mechanical and metallurgical characterization study of FSW of 3 mm sheets of AA6061-T6 with AA6082-T6 was conducted by [Moreira et al., 2009]. Plates were friction stir welded as similar alloys and also dissimilar alloys. Speeds of 1120 rpm and 224 mm/min at 2.5° tilt angle were used. Threaded 5 mm diameter tool with 17 mm shoulder diameter was used. The friction stir welding of the plates was performed along the rolling direction. Microstructures and micro hardness of similar alloys were performed. A decrease in hardness values was observed when approaching the thermodynamic heat affected zone for both alloys. The average hardness values of the stir zone (SZ) were found to be lesser than the hardness of the base alloy. The transition between thermodynamic heat affected zone and heat affected zone outside the nugget exhibited a lower hardness values. The difference of the micro hardness values in the welded area and base material was ascribed to the difference between the microstructures of the base material and welded zone. Micro hardness profile formed "W" shape profile for both alloys.

2.6 Fatigue tests

2.6.1 Fatigue tests on AA5XXX

An investigative study of fatigue and fracture behaviours of FSW and friction stir processed (FSP) joints of AA5083-h111 was embarked upon by [Hussein and Al-Shammari, 2018]. The work aimed at understanding the mechanisms involved in fatigue and crack initiation of welded AA 5083 joined by FSW and FSP. A 3mm thick plate was FSW by tool steel of shoulder diameter of 18 mm, 5 mm diameter tapered pin and 2.9 mm in length. For FSW, the rotational speed of 1500 rpm, and traverse speed of 20 mm/min were used while rotational speed of 1500 rpm, traverse speed of 40 mm/min was used for FSP. An alternating bend loading was used for fatigue tests. Uniform amplitude was set where the stress ratio was $R = -1$. Two tested samples were done at each load condition. Specimens were cut at direction perpendicular to the weld line of friction stir welded and processed plate to perform the test. A fatigue limit of over 2×10^6 for FSW and 3×10^6 cycles for FSP and base metal was considered a run-out test. Specimens for fatigue testing were rectangular in shape (89 mm x 10 mm) where the centre of welded joints were at offset distances of 59 mm from one end. From S-N curves it was observed that parent material specimen achieved an endurance limit of 86.388 MPa, FSP specimen achieved 81.089 MPa while FSW only obtained 71.869 MPa. The study also observed that the cracks initiated on the weld regions for both FSW and FSP specimens.

2.6.2 Fatigue tests on AA6XXX

A fatigue test was conducted on compact tension (CT) specimens by [Moreira and Jesus, 2008]. The study was done on FSW AA6082-T6 to investigate the fatigue crack growth propagation of the specimen. The FSW joints were performed using the rotational speed of 1500 rpm traverse speed of 800 mm/min at a tilt angle of 2° . A tool with 15 mm shoulder diameter and a 6 mm diameter threaded pin was employed. Three specimens were prepared from the FSW joint. First one was cut on the heat affected zone, the second was cut along the welded joint on the nugget and the third one was on the traverse orientation of the welded joint. Experiments were conducted on constant load amplitude 20 Hz frequency. Crack propagation was monitored through visual measurements with aid of a travelling microscope. After fracture, for the first specimen there were no visually distinguishable particular features. With the second specimen the weld bead was characterized by striations related to the tool path. For last specimen, different zones were recognizable. The heat affected zone was present, but when the crack reached the thermo-mechanical affected zone onion rings were visible.

2.6.3 Fatigue test on dissimilar alloys

A comparative study between microstructure and mechanical properties of dissimilar aluminium alloys by FSW was conducted by [Sarsilmaz, 2017]. An 8 mm plates of AA2024-T3 and AA6063-T6 aluminium alloys used where AA2024 alloy was placed

on the advancing side and the AA6063 alloy was on the retreating. Combination speeds used were 900, 1120 and 1400 rpm together with 125, 160 and 200 mm/min. the tool used was D5 steel with conical triangular pin geometry tilted at 2.5° angle. Specimens were prepared in accordance with ASTM E-466 standard. The stress amplitude $\Delta\sigma$ (MPa) versus the corresponding number of cycles scenario was set in a sinusoidal load–time function. A tensile stress was applied axially with a frequency ranging from 100–130 Hz. The applied stress amplitudes were from 25 MPa to 110 MPa for the nine different types of welding conditions to get fatigue lifetime between 1×10^3 and 1×10^6 . In different welding speeds, the number of cycles to failure increased with increasing stress amplitude. The good results were recorded at the joint FSWed at 900 rpm and 200 mm/min as 45 MPa while the poor results were as 29 MPa at 1400 rpm and 125 mm/min.

A fatigue experimental study of FSW of AA5083-H111 and AA6082-T651 was conducted by Gungor et al., (2014b). An H13 tool steel with 20 mm shoulder, tapered cylindrical pin was used. The pin was 8mm in diameter and 5.7mm long. Rotational speed was 1250 rpm traverse speed of 64 mm/min at 2° tilt angle was set. Similar joints were also welded and tested for fatigues. Yield stresses were used as a determinant for fatigue test settings. During fatigue test, the joint AA5083-H111/AA6082-T651 exhibited better fatigue limit than AA6082/AA6082 joint. Crack propagated from stir zone and proceeded to thermos-mechanical affected zone. The fatigue limits of the joints had achieved different strength to each other. The difference of fatigue limits of the joints was attributed to the difference in tensile strengths.

2.7 Fractography by Scanning Electron Microscopy (SEM) on dissimilar alloys

Tensile tests are normally performed in dissimilar joints with the purpose of analysing their tensile properties. The post tensile tests specimens are normally used to analyse the failure mode occurred at the joints. This section is reviewing literature that involves the analysis of the fracture analysis of the FSWed dissimilar aluminium alloys.

2.7.1.1 Fractography of AA5XXX

An investigative study of FSWed joint of AA5083/AA5083 was examined using scanning electron microscope (SEM) by [Ahmed et al., 2017]. The study evaluated the nature of fracture after tensile test for the said alloy. The 6 mm thick plate was friction stir welded in similar butt joints. Constant tool rotational speed of 300 rpm was combined with four traverse speeds of 50, 100, 150 and 200 mm/min. A tool had 18 mm shoulder diameter with a concave face. The pin had a length of 4.8 mm with smooth taper cylindrical geometry and was tilted at 3° angle during FSW. Friction stir welded joint was cut in traverse orientation. The cross-head speed of 3.6 mm/min was used during the tensile testing. On the SEM images, it was observed that the topographies of the fracture in 50 and 200 mm/min indicated a mixed ductile-brittle fracture patterns. This was also characterised by the presence of dimple structure and smooth facets. The dimple sizes ranged from 7–25 μm . The size of dimples was accredited to high deformation during friction stir welding process which led to the strengthening the nugget zone in relative to the AA5083 parent material. The 100 and

150 mm/min images showed excessive voids and tool striations which explained the lower values in tensile strengths.

2.7.1.2 Fractography of AA6XXX

Chen et al., (2017), performed SEM fractographs from three specimens which were the parent material and two FSW joint specimens. The FSW joint was cut in two directions transverse and longitudinal FSW specimens. The specimens were from plate of AA6061 which was FSWed at 1000 rpm and 20 mm/min. The tool used had a shoulder of 25 mm, a pin diameter of 8 mm and 6.35 mm long. All three specimens were tensile tested at crosshead speed of 3 mm/min. The traverse specimen failed on the heat affected zone while parent and longitudinal failed on the centres. Tensile test results showed that both traverse and longitudinal AA6061-AA6061 had necking deformation except for the parent material AA6061. The SEM fractographs showed dimple fracture configurations with teared edges full of micropores. The dimples were of different shapes and sizes. Comparing longitudinal specimen of AA6061-AA6061 and traverse AA6061-AA6061 were characterized by deeper dimples and thinner teared edges. The study concluded that the longitudinal AA6061-AA6061 had much better mechanical properties than the parent material AA6061. It was also observed that the FSW specimens cut longitudinally had much better mechanical properties than did the specimens cut in traverse direction.

SEM observations were conducted to reveal fracture surfaces by [Patil & Soman, 2014]. The study investigated the effect of tool geometry and welding speed on mechanical properties and microstructure of FSW joints of AA6082-t6. Three different tool pin geometries were used that is tapered cylindrical four flutes, triangular and hexagonal. Rotational speed ranged from 1600 -1650 rpm, traverse speed ranged from 30 -74 mm/min. All the tools were having shoulder diameter 18 mm and pin length of 4.6 mm tilted at 0° angle. Fractured tensile tested specimens were analyzed at high and low magnifications to determine the fracture patterns. For triangular and hexagonal pins, the fracture surfaces under SEM were characterized by very fine dimples which was ascribed to ductile behavior of the material before failure. In four flute pin, cleavage cracking was most easily identifiable transgranular brittle fracture in FSW joint.

Moreira & Jesus, (2008) analyzed compact tension (CT) specimens using SEM. The study analysed the fatigue crack growth behavior of the FSW AA6082-T6. The FSW joints were performed using the rotational speed of 1500 rpm traverse speed of 800 mm/min at a tilt angle of 2°. A tool with 15 mm shoulder diameter and a 6 mm diameter threaded pin was employed. Three specimens were prepared from the FSW joint. First one was cut on the heat affected zone, the second was cut along the welded joint on the nugget and the third one was on the traverse orientation of the welded joint. On the first specimen, the crack surface became rougher along the crack lengths. With higher magnification, fractographs had faded fatigue striations and voids. The second specimen was characterized by the striations which corresponded to the tool advance per revolution. The crack surface was found to be different in the two different zones of each striation marks. On the traverse specimen, the TMAZ, had a topography which corresponded to the material flow during FSW process. The layers of material flow at the weld zone easily recognized.

2.7.1.3 Fractography of Dissimilar alloys

Selamat et al., (2015) investigated SEM fractures mechanisms of dissimilar alloys AA5083 and AA6061. Plates were butt FSW of rotational speed of 1000 rpm and the traverse speed of 100 mm/min. The tool was made of H13 tool steel tilted at angle of 3°. After the joint was FSWed, tensile specimens were cut and tested at a displacement rate of 2.4 mm/min. During FSW, AA6061 was placed on the retreating side. AA6061-AA5083 showed a fracture surface that was covered with dimples and voids with varying depths and sizes. This nature of fracture was associated with ductile behaviour and the formation of necking before fracture. The shallow dimples were found surrounding the transgranular fracture surface. Shallow dimples concurred with the limited elongation during the tensile test with no necking found on the samples.

FSW AA5083-H321 and AA6061-T6 were analyzed under SEM by [Devaiah et al., 2017]. The study looked effect of welding speed on mechanical properties of dissimilar FSW aluminum alloys. A constant tool rotational speed of 1120 rpm and four different traverse speeds 40, 63, 80 and 100 mm/min were employed. A H13 tool steel with cylindrical taper threaded pin geometry and a scrolled surface concave shoulder was used. The tool had a shoulder diameter of 18 mm with a pin diameter and a length of 6 mm and 4.7 mm respectively. After fractured tensile tests, fractography was conducted. Fractographies were characterized by dimple pattern on the whole width of the specimen. All joints were broken on the retreating side during tensile testing where hardness values were the least. The joints fabricated at the condition of tool rotation speed at 1120 rpm, tool tilt angle 2.5° and traverse speed at 80 mm/min exhibited higher ductility as compared with other speed combinations. This was attributed to a presence of small shallow dimples. This was also accredited to the high plastic deformation which showed the more intense ductile fracture.

Gungor et al., (2014b) examined FSW joint of 5083-H111 and 6082-T651 aluminum alloys by SEM. The study was evaluating the mechanical, fatigue and microstructural properties of the alloys. Rotational speed of 1250 rpm tool and traverse speed of 64 mm/min at tilt angle of 2° used. Fractured surfaces of the fatigue joints were characterized by coarse dimples while fractured tensile joints had clustered fine dimples as indication of ductile behavior.

Palanivel et al., (2014) conducted SEM experimental study on mechanical and metallurgical properties of dissimilar FSW AA5083-H111 and AA6351-T6. The tool had a shoulder diameter of 18 mm, 6 mm pin diameter with a pin length of 5.7 mm. The tool was made from high carbon and high chromium steel with straight square pin. AA6351-T6 was placed on advancing side and AA5086-H111 on retreating side of the joint line. Uniform rotational speed of 950 r/min and three different travel speeds of 36, 63 and 90 mm/min were employed. Specimens were cut on the traverse orientation of the FSW joint for tensile testing. The fractured surface for 63 mm/min of the tensile tested dissimilar weld specimens was analyzed. The fracture surface exhibited a dense population of microscopic voids that varied in size and shape. The failure of the dissimilar joint was dominated by the coalescence of those microscopic voids. The observed failure pattern was ductile fibrous fracture in nature. Lower traverse speed (36 mm/min) gave rise to higher heat conditions which led to the coarseness of grains. Lower speed was also suspected of causing improper mixing of material which caused reduced UTS. The higher traverse speed (90 mm/min) caused insufficient stirring. The material on the advancing side of the tool did not travel enough to the retreating side

which caused voids. Improper mixing of the material was also attributed to lower heat generation to melt the material and also faster cooling rate.

2.8 Classification of FSW for dissimilar aluminium alloys

Mishra, (2018) classified the FSW of dissimilar alloys into three categories namely:

- FSW of dissimilar alloys having widely different melting point
- FSW of dissimilar alloys with similar base metals and melting point
- FSW of different alloys having dissimilar base metals and similar melting point

2.8.1 FSW of dissimilar aluminium alloys with widely different melting point

Mishra, (2018b) explained that this category refers to the dissimilar metal welding where the base metal of the alloy differ from each other entirely and have wide difference in their melting point. The typical example for this category will be the welding of Al/Mg alloys to Cu/Ti/ferrous alloys.

Welding of alloys using various methods always proved to be a challenge. Welding of alloys brings problems of development of brittle intermetallic compounds, as well as the development of low melting point eutectics. In some alloy systems like aluminium to magnesium both problems exist. Wide differences in melting points poses complications. Aluminium to copper for electrical conductors was reportedly to have been successfully welded, even though additional refinement is advised before commercial exploitation can occur [Gordon, 2010].

Chaudhari, (2014) studied mechanical properties of FSW Aluminium 6082 to copper. The study was aimed at analysing the effect of the microstructures and mechanical properties of FS welded joint of 6082 aluminium alloy and pure copper. It was found that friction stir welding is the most suitable technique of joining dissimilar alloys among all techniques and that they are suitable for engineering structures. Chaudhari, (2014) agrees with Mishra, (2018) that aluminium and Copper are widely applied in engineering structure due to unique performances such as higher electric conductivity, heat conductivity, corrosion resistance and mechanical properties. However, the melting points of both materials have a significant difference.

Al-Jarrah et al., (2014) conducted a study on surface morphology and mechanical properties of aluminium-copper joints welded by FSW. The probe was offset with respect to centre of butt line. A defect-free welded joint was produced by arranging Al either on advancing or retreating side with sufficient probe offset to Al side.

2.8.2 FSW of dissimilar alloys with similar base metals and melting point.

This category is vast as include a number of alloys such Al – Al alloys, Mg – Mg alloys and Ferrous – Ferrous alloys where the base materials remain same and they differ only in terms of major alloying elements and their concentrations.

Mishra, (2018a) friction stir welded a 5 mm thick plates of AA5052 and AA6061 aluminium alloys. A cylindrical high speed steel tool of 25 mm shoulder diameter, 4.8 mm tool pin length and 6 mm diameter tool pin was used at 3° tool tilt angle. Tool rotational speed of 1120 and 1400 rpm were used with changing traverse speeds of 60, 80 and 100 mm/min. AA5052 was placed on the retreating side while its counterpart was on the advancing side. The study aimed to analyse the forces exerted at different speed combination and effect thereof. It was observed that at 1400 rpm speed the load decreased as compared to 1120 rpm even to halve the load. Torque was also noted to decrease with increase in rotational speed and the torque was not affected with variation in traverse speeds. Welded joint showed wavy and distorted appearance. The serrated joint line appeared along the thickness of the weld. Joint line was considered imperfect and was also termed as “joint-line remnant”. A sudden shift across the AA5052- AA6061 boundary in the stir zone was observed. The micro hardness values were slightly uniform in the stir zone and the adjacent heat affected zone for both the aluminium alloys. Outside the heat affected zone into the parent material region, there was a smooth transition of the micro hardness to the base material micro hardness values decreasing from the higher hardness in the nugget at the AA6061 side and increasing from lower hardness in the stir zone at the AA5052 side.

2.8.3 FSW of different alloys with dissimilar base metals and similar melting point

This category is mainly for dissimilar Friction Stir Welding of alloys such AZ31B Magnesium alloys and Aluminium alloys and similar combinations.

Morishige et al., (2008) studied dissimilar welding of Al and Mg Alloys by FSW. AZ31B magnesium alloy and A5052 aluminium alloy of 3 mm plates were butt FS welded. Rotational speeds used were 800, 1000, 1200, 1400 and 1600 rpm and traverse speeds of 100, 200 and 400 mm/min, respectively. A JIS SKD61 with shoulder diameter of 12 mm, pin diameter of 4 mm and length of 2.9 mm were set at uniform tool tilt angle of 3°. The highest ultimate strength and elongation, were recorded by the joint welded at 1000 rpm and 200 mm/min with a joint efficiency of 61% of the strength of the base material (AZ31B).

Mishra, (2013) reported that magnesium alloys are weaker than aluminium alloys in terms of their average strength. Thus, welding of dissimilar magnesium alloys in itself offers little or no challenge. So, the tools used for welding aluminium alloys can be used for magnesium alloys without worrying about tool wear.

Çam, (2011) clarified that Mg-alloys have non-symmetrical hexagonal crystal structure which helps to able cold working which increases with increasing temperature. The workability of Mg-alloys assists a lot in FSW as these alloys are readily plasticised at the temperatures obtained during welding. Even ordinary cylindrical tools with threads made of tool steels (e.g. H13) similar to one used in FSW of Al-alloys could also be used for FSW Mg-alloys.

Singh et al., (2018) in their review on friction stir welding of magnesium alloys affirmed that the FSW of magnesium alloys are used in land transportation, aerospace, railway, shipbuilding and marine, construction, and more other industrial applications. Magnesium alloys can also be used in industrial equipment of nuclear energy because

magnesium alloys have low tendency to absorb neutrons, sufficient resistance to carbon dioxide and excellent thermal conductivity.

2.9 Effect of specimen location on the welded plates

A study was conducted by Doude et al., (2015) on optimizing weld quality of a friction stir welded aluminium alloy. Different tool rotational speeds of 150, 200, 250, 300, 400, 500, 600, 700, 800, 900 and 1000 rpm and travel speeds of 100, 150, 200, 250, 300, 350, 400, 450 and 500 mm/min were used. A 6.35 mm thick AA2219- T87 panels were cut to 100 mm × 610 mm in dimensions. A total of 50 specimens with a width of 12.5 mm were cut over a distance of 500 mm. First specimen was cut at 50 mm from the start of the weld, thirteenth specimen was at 220 mm while the last specimen was cut at 440 mm from start of the weld. The study observed that irrespective of the specimen location from the starting point it did not have effect on results

Ravindar and Gururaj, (2015) presented a results where the constant rotational speed of 800 rpm and variable traverse speed 60, 70 80 mm/min were used. Tensile test specimen broke in similar fashion regardless of the location where the specimen was sampled.

Nadim and Ahmed, (2014), presented results of a study between AA 6061-T6 and AA 5083-H1111-O where two (round and square) different tool pins were used. Rotational speeds of 500, 700 and 1000 rpm were used against a constant traverse speed of 25 mm/min. Two specimens were sampled per speed combination for tensile and hardness testing at different location of the plate. Results did not show any significance due to sample location.

Magee et al., (2017) presented a study where a rotational speed of 800 rpm and traverse speed of 88 mm/min were used on AA 6061-T6511 3 mm thick plate. Both plates were 150 mm long and 50 mm wide friction stir welded by threaded step spirals pin. Four specimen were extracted on different locations of the plate as (37, 60, 100 and 130) mm from the edge of the plate. Specimen at 37 mm had the least strength followed the last specimen, where the third specimen showed greatest strength compared to all of them.

2.10 Summary

Literature review in this chapter has covered development in FSW. The focus was on dissimilar friction stir welded of aluminium and other alloys. The study also touched on specimen extraction location post FSW, parameters affecting FSW and subsequently properties obtained.

Aluminium alloys 5083 & 6082 are able to be friction stir welded together in their different temper designations. Friction stir welding is only possible if two materials to be FS welded are of the same thickness. Harder material of the two is recommended to be placed on the advancing side for better mixing during friction stir welding process. The use of converted milling machine is among the affordable methods of conducting friction stir welding with minimum cost for most researchers.

Different tool materials are able to friction stir weld aluminium alloys, and the most used being the H13 tool steel for its machining affordability and its strength. Different geometries do affect the outcome of metallurgical integrity of the joints, but most used tool geometries are round, square and triangular shapes with threads for better mixing and forging of the material along the joint.

Tool rotational and traverse speeds have been used. What is notable is that slow tool rotation and traverse speeds tend to cause more unnecessary heat input while to fast speeds cause the minimum heat generated which causes lot of defect due to cold friction stir welding. Most of researchers obtained better results on combinations speeds of 600-1000 rpm and 60 -100 mm. The ratio of tool pins to tool shoulders also proved to be of importance. The general recommended ratio of tool pin to tool shoulder is 3:1 for better heat input.

Most of the plates friction stir welded are shorter in length (most 150-200 mm) but for this study a longer length will be used to evaluate the effect of specimens extracted from different locations along the welded joint. It was also noted that most studies evaluate the effect of different speeds combinations but for this study same speed combination will be employed but both materials will be placed on advancing and retreating side.

Chapter Three: Experiment Setup

3.1 Introduction

This chapter describes the equipment used in performing experiments for this study. It further describes the welding machine used to produce the welds. The techniques used to analyse the welded joints are also given with details in this chapter. The welding parameters used in producing welds are also given in this chapter.

3.2 Welding Set-up

The following equipments were used in producing the welds suitable for this study:

1. True Mechanical Shearing machine
2. Tri-flat pin tool
3. Clamps with backing plate
4. Milling machine

3.2.1 Mechanical shearing machine

The truecut mechanical shearing machine QH11D-3.5 x1250 shown in figure 3.1 is used in cutting/shearing of metal plates and metal sheets into required sizes by means sharp hardened blades. The machine allows a plate thickness of 3.5 mm thickness and 1250 mm width. The plate/sheet is positioned horizontally on the bed and against the reference edge and pushed against the measuring stopper. Once the foot brake is pressed, the clamps hold material in position and blades would descend to cut material as required.

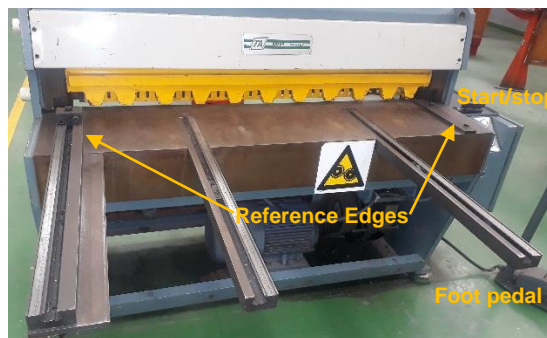


Figure 3.1: Truecut Mechanical Shearing machine QH11D-3.5 x1250

3.3 Milling machine

The Lagun FU. 1-LA milling machine in figure 3.2 is a machine with a vertical or horizontal spindle that rotates a tool above a horizontal table. Horizontal table is able to travel up, down, toward the machine or outwards the machine. The tool does not move but only rotates and tilts at a required angle. Milling machine can be fully automated like computer numerical control (CNC) or manual semi-automatic operated. Milling machine was fitted with slotted milled mild steel backing plate of 800 mm x 130 mm x16 mm which used to clamp plates. Eight clamps were used to secure plates onto the backing plate. Backing plate was aligned and fixed on the milling table. The Lagun FU. 1-LA was a semi-automatic milling machine capable of feeding automatically on

the set tool rotational and traverse speeds. It also able of achieving variable tool rotational speed of 0 – 1800 rpm, table traverse speed of 0 – 100 mm/min and the head achieving 360⁰ turn.

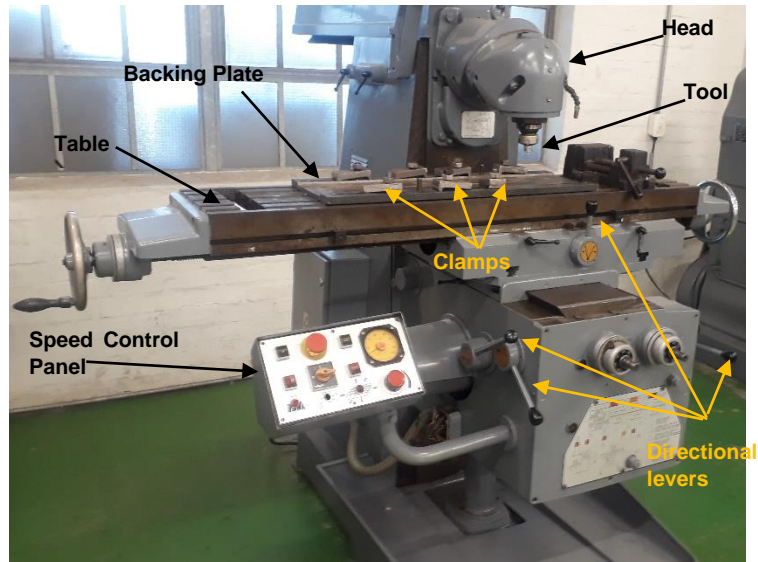


Figure 3.2: Lagun FU. 1-LA milling machine

3.4 Welding performance

Dissimilar aluminium alloy plates were prepared before the FSW was performed.

3.4.1 Preparation of plates

The 6 mm thick aluminium alloys 5083-H321 and 6082-T651 were cut using the truecut mechanical shearing machine as shown on figure 3.3. The dimensions used were 600 mm long and 70 mm wide and these dimensions were designed to fit into the back plate. The length of the plate was designed to allow considerable gaps between specimens during specimen sampling.

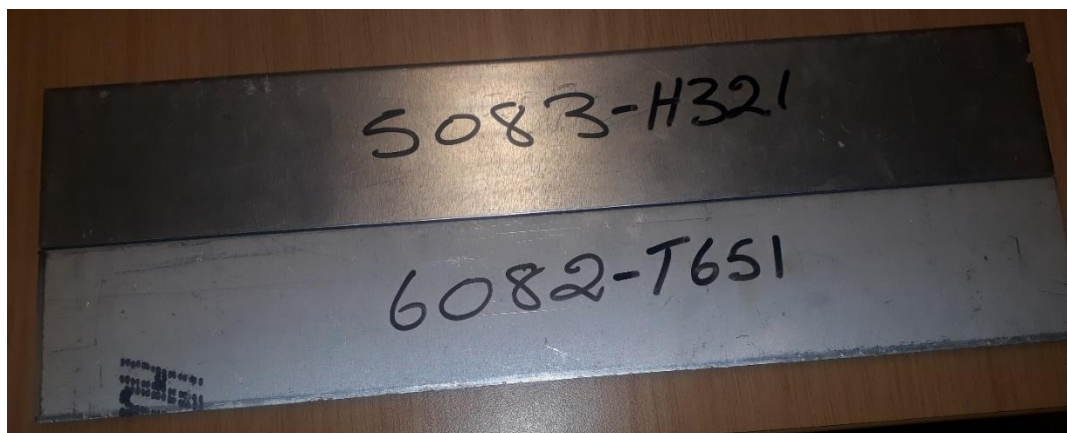


Figure 3.3: Prepared plates for FSW

The edges of the plates after cutting were clean and free of burrs.

3.4.2 FSW setup

FSW was done on plates of 5083-H321 and 6082-T651 dissimilar alloys. Plates were positioned and clamped onto the backing plate with no gap between the interfaces. Aluminium alloy 5083-H321 and 6082-T651 were placed on the advancing and retreating sides respectively. Figure 4 shows how the plates were clamped and descending of the tool to position before FSW. Plates were only cleaned with a dry cloth before welding. Tri-flat grooved H13 tool steel was used. The tool pin had a hardness of Rockwell C of 52HRC.

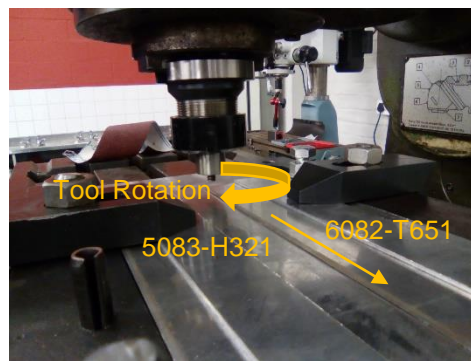


Figure 3.4: Welding Setup

Figure 3.5 presents the tool used in the study. The tool pin is triflat with grooves H13 tool steel. Tool pin found on the literature are cylindrical threaded, cylindrical smooth, square profiled, triangular profile with threads.

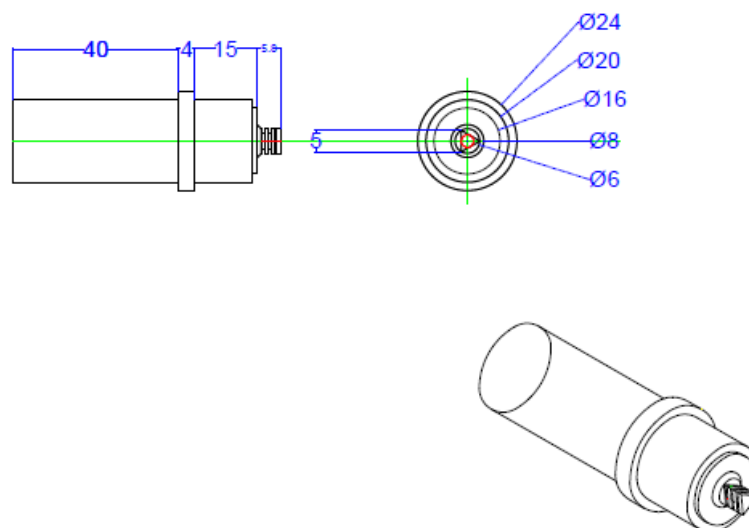


Figure 3.5: Tool geometry (all dimensions are in millimetres)

Parameters used are shown on table 3.1.

Table 3.1: Friction Stir Welding Parameters

Parameter	Sample 1	Sample 2
Tilt Angle, Θ ($^{\circ}$)	2	2
Tool Rotational Speed (rpm)	800	800
Traversing Speed (mm/min)	60	60
Dwell time (seconds)	30	30
Plate thickness (mm)	6	6
Plunge depth (mm)	5.8	5.8
Shoulder diameter (mm)	20	20
Pin diameter (mm)	6	6
Positioning of alloys	5083-H321 on advancing side & 6082-T651 retreating side	6082-T651 on advancing side & 5083-H321 retreating side

3.5 Sample preparation

Equipment used for preparation of samples were electrical discharge machine, hot mounting press and polishing machine.

3.5.1 Electrical discharge machine (EDM)

EDM Accutex AU-500iA wire-cut in figure 3.6b is a machine that is using electrical charged brass wire to cut only electrical charging objects like metals. The wire runs continuously between two spools (figure a and c). A small hole is drilled on the work piece outside the cutting path to initiate wire-cutting. Material is clamped in position and the drawing was loaded into EDM for profile cutting. The work piece is submerged under water during cutting process. The water helps in flushing away cut debris and cooling the work piece to prevent residual stresses during cutting process.



Figure 3.6: (a) Inside spool and specimen table, (b) EDM Accutex AU-500iA wire-cut and (c) hidden spool and brass wire

3.5.2 Hot Mounting Press

In preparation of metallography, Struers LaboPress-3 hot mounting press in figure 3.7 is used. Hot mounting press uses elevated temperature to put a mould around small specimens so that they can be handled. Hot mounting uses only powder that is suitable for hot moulding. Mounting is when the facing down specimen is put into the cylinder of the mounting press. The Bakelite powder is poured into the mounting press cylinder. The mounting press is set to required force, heat and cooling time for the entire process. Mounting press cylinder is closed, water tap for cooling is open and the machine is started. Once the entire duration lapse, the cap is opened and the plunger inside the cylinder is raised up to release the moulded specimen. The whole process is automatically.



Figure 3.7: Struers LaboPress-3 hot mounting press

3.5.3 Polishing machine

Struers LaboPol 5 polishing machine in figure 3.8 was used for polishing of specimens. Polishing is performed so as to reveal metallographic characteristics under metallurgical microscope and micro-hardness tester. Etching agent is also used timeously until grains or metallurgical zones are revealed.



Figure 3.8: Struers LaboPol 5 polishing machine

3.6 Specimen preparation

The samples were cut in different locations from the welded plates [see figure 3.9]. First specimens were taken from a distance of 100 mm from the beginning of the weld. Second specimens (middle of the weld) were taken at a distance of 300 mm and the end of the weld specimens were taken at 500 mm from the beginning of the weld. The wire cut was used in cutting all the samples and this cutting technique was chosen because it does not involve temperature variation during its operation.

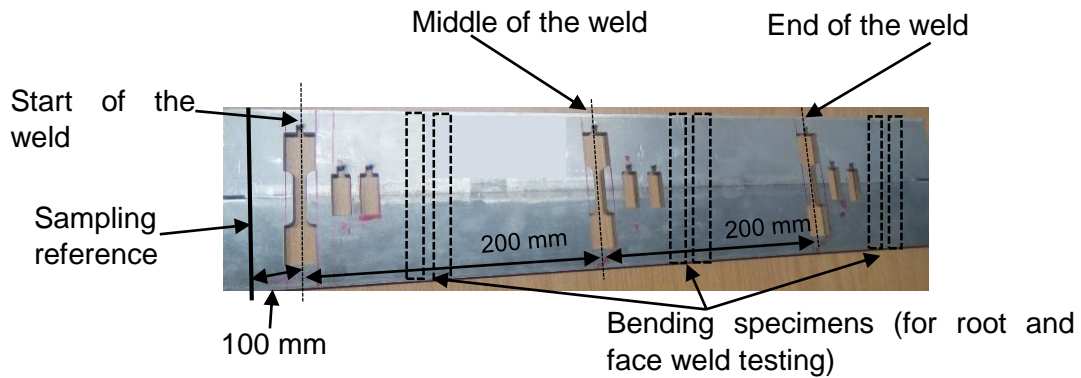


Figure 3.9: Sample positioning

3.6.1.1 Tensile test specimen cutting

ASTM E8M-04 sub-size specimen was used as a guide to determine the shape and dimensions of the specimens.

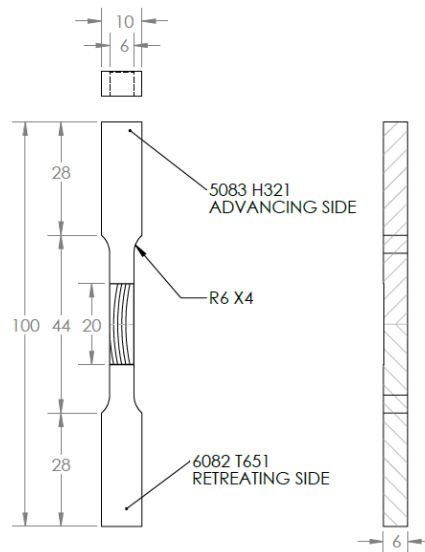


Figure 3.10: CAD drawings for tensile test specimens (dimensions are in mm)

Three sets of tensile specimens were prepared as follows:

- (a) A specimen for each of parent materials
- (b) Three specimens of 5083-H321 on advancing side
- (c) Three specimens of 6082-T651 on advancing side

3.6.1.2 CAD drawings for metallographic specimen cutting

Three sets of specimens were prepared for micro-hardness, microstructure and macrostructure as follows:

- (a) Three specimens of 5083-H321 on advancing side, sampled at start, middle and end of run. Parent materials were also measured 12 mm from centre of the weld joint, figure 3.11a.
- (b) Three specimens with 6082-T651 on advancing side, sampled at start, middle and end of run, figure 3.11b.

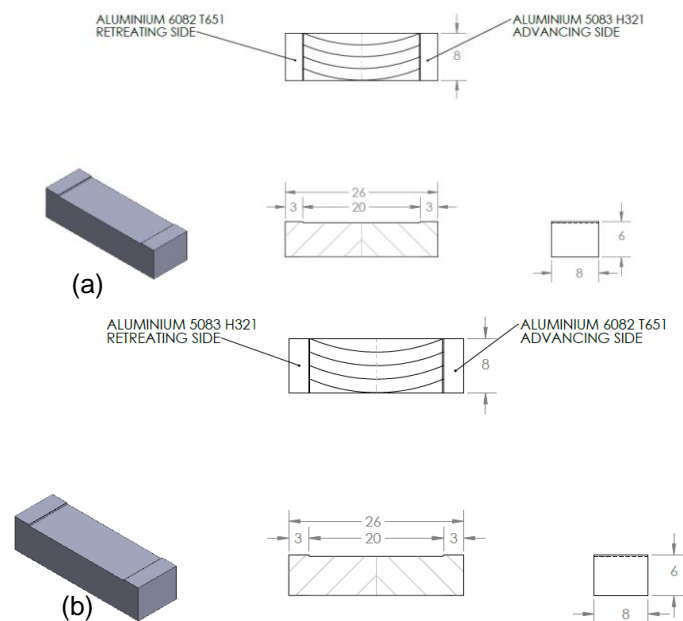


Figure 3.11: CAD drawing for metallography and micro-hardness specimens

3.6.1.3 Bending specimen cutting

Bending specimens were cut across the weld joint as shown in figure 3.12.

Five sets of bending tests specimens were prepared as follows:

- (a) One of each parent materials that is 5083-H321 and 6082-T651.
- (b) Three for face bending (this means that actuator is pushing direct opposite the top face) when 5083-H321 was on advancing side, sampled at start, middle and end of run.

- (c) Three for root bending (this means that actuator is pushing direct opposite the bottom face) when 5083-H321 was on advancing side, sampled at start, middle and end of run.
- (d) Three for face bending when 6082-T651 was on advancing side, sampled at start, middle and end of run.
- (e) Three for root bending when 6082-T651 was on advancing side, sampled at start, middle and end of run.

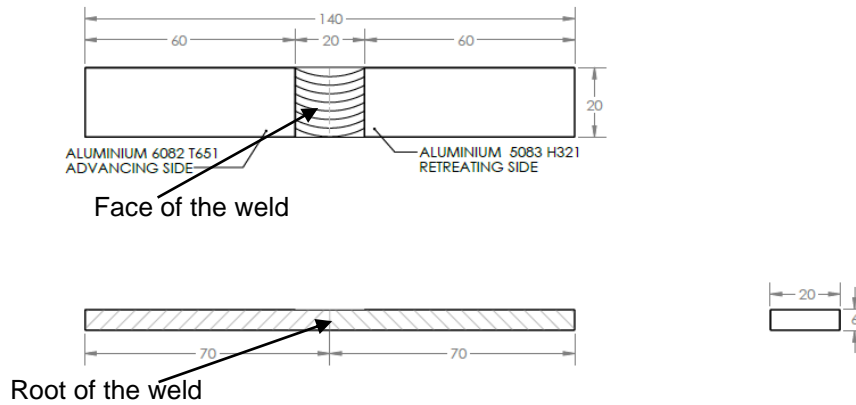


Figure 3.12: CAD drawings for bending test specimens

3.6.2 Mounting and polishing of specimen

Struers LaboPress 3 was used to mount specimens for metallography. Specimens were ready for polishing and etching. Specimens were allowed to set and Bakelite around the edges of specimen shown good adhesion as seen in figure 3.13.

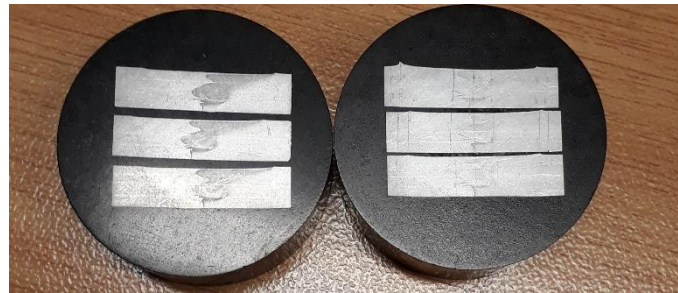


Figure 3.13: Specimens after mounting

Specimens (Micro-hardness, microstructure and macrostructure) mounted in a Bakelite resin were mounted on the Struers LaboPol 5 polishing machine. Initially, specimen were grounded on the Akasel piano 220-grit to flatten them and also to expose the area to be tested. After polishing, the samples were etched using a Keller etchant to reveal the microstructure. Under MET microscope grain boundaries were not visible and further polishing was conducted as shown on the table below.

Table 3.2: Alternative polishing steps used for Al-Alloys

Step	Pad	Polishing solution	Time
Plane Grinding	2000 grit SiC	Water	5 min
Fine Grinding	4000 grit SiC	Water	5 min
Polishing	Moran	6 μm	5 min
Polishing	Nap	1 μm	10 min
Polishing	Nap	0.25 μm	5 min

The extended time needed on the 1 μm polishing step was due to the skipping of the 3 μm polishing step (on the Daran Pad). In an ideal situation the final step would use 0.2 μm colloidal Silica solution (on the Chemal pad) but in lieu of that 0.25 μm Diamond polishing solution was used.

The colour etchant used to determine microstructure and grain boundaries is known as Weck's Reagent. Weck's Reagent is made by dissolving 1 g of NaOH pellets in 100 ml of distilled water and then mixing 4 g of KMnO_4 into the solution. The sample was immersed in the etchant for 15 seconds and then thoroughly rinsed with distilled water. Afterwards ethanol was used to clean the surface which was then dried using hot air.



Figure 3.14: Etched Specimens

Specimens for micro-structured were prepared successfully and the areas for testing were clearly exposed. Figure 3.14 (a) is when 6082-T651 was on advancing side and over etching was observed and figure 3.14 (b) is when 5083-H321 was on advancing side.

3.7 Equipment used for tests

To perform different tests, different types of equipment were considered. Tensile testing machine was used for tensile tests and bending tests, metallurgical microscope was used for macrostructures and microstructures while the computerized micro-hardness tester was used for micro-hardness specimens. Liquid penetrant testing (LPT) method was used to verify cracks on bending specimens after bending test. SEM was used to characterize the nature of failure after tensile tests.

3.7.1 Tensile testing machine

Hounsfield Tinius Olsen H50KS machine shown in figure 3.15 is a machine with two stationary and movable jaws/grips. Stationary jaws/grips are fixed on the base of the frame of the machine. Cross head is attached on the mechanical screw operated frame. Once the specimen is clamped a movable grips would pull the specimen until it breaks or to a defined extension or load. In case of compression/bending the grips on the crosshead would push as required. Dimensions of the specimen and testing parameters are recorded into the software. The software controls, records information as testing is progressing and do data processing. Load cell and extensometer are fitted to record force and elongation of the specimen respectively. Serrated faced grips are used to avoid specimen slippage during testing.

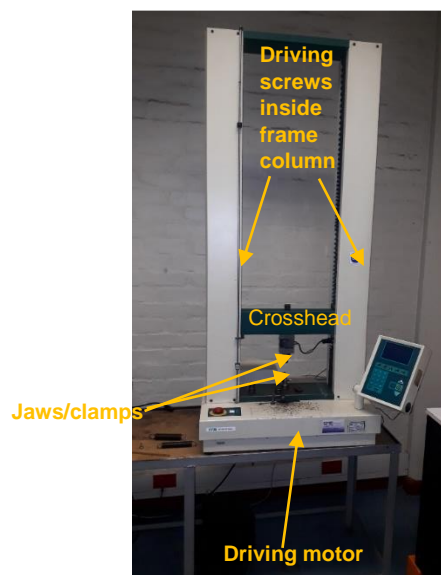


Figure 3.15: Hounsfield Tinius Olsen H50KS machine

3.7.2 Liquid penetrant test (LPT)

Liquid penetrant test (LPT) is applied as non-destructive test (NDT) to reveal possible defects such as cracks. This NDT is applied on the surface of nonferrous and ferrous metals with the exception of porous metals like cast iron, etc. LPI method uses solvent, penetrant and developer as shown in figure 3.16.

Surface is cleaned using solvent cleaner with the aid of cloth. Surfaces is allowed to dry for few minutes. Penetrant is then applied and kept for longer period approximately ten minutes. Solvent cleaner is applied on the surface. Cloth is used to remove penetrant on the surface. Developer is applied on the surface to draw the penetrant to promote capillary action. Developer is then removed from the surface using a cloth. Where there are cracks lines will emerge on the surface.



Figure 3.16: Liquid Penetrant Test kit

3.7.3 Metallurgical light microscope

Metallurgical inverted AE2000 MET microscope in figure 3.17 is an equipment that uses an illuminator, reflector and objective to bring light image of the opaque specimen to the eye piece/ screen. Specimen is placed on the stage and different objectives are fitted to enable magnification of light image. In an inverted microscope objectives bring light from the bottom of the specimen. Once the image is focused a photograph will be captured for analysis such as grain size, microstructure, etc. Three dimensional adjustments can be achieved.

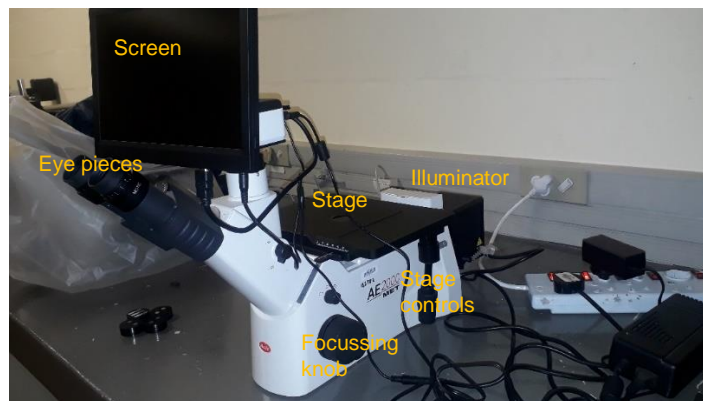


Figure 3.17: Metallurgical inverted AE2000 MET microscope

3.7.4 Microhardness

Vickers microhardness services were outsourced. Generally, microhardness as seen in figure 3.18 is a machine that uses an indenter to exert small amount of force to make indentations for analysis. Specimen is positioned on the working table, force is set and indenter makes a dent. Indenter is moved away and camera is brought onto the dent by turning the turret. Dent is captured on the screen for measurements.

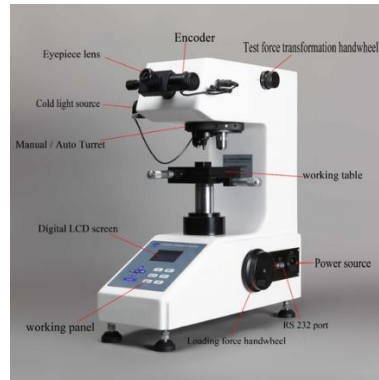


Figure 3.18: Vickers microhardness tester [source: Kamm & Voort, 1939]

3.7.5 Scanning Electron Microscope (SEM)

Scanning electron microscope (SEM) was outsourced. Basically, SEM works similar to light microscope except that instead of light, SEM use high beam electrons to reflect light from the specimen in a higher resolution. Specimen is positioned inside the glass chamber. SEM takes limited dimension sizes though it could take number of specimens at once. Figure 3.19 presents samples that were used as marked in red.

On Figure 3.19a 6082-T651 was on advancing side while on figure 3.19b 5083-H321 was on the advancing side.

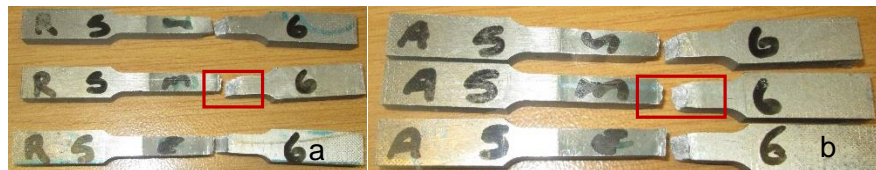


Figure 3.19: Sampling of SEM specimens

3.8 Performance of tests

This section describes different methodologies used in conducting tensile, bending, LPT, microhardness, microstructure/macrostructure and fractography tests.

3.8.1 Tensile testing

A Hounsfield Tinius Olsen H50KS, tensile test machine on figure 3.20 was used. 50 kN load cell was used to record the force. The specimen had a gauge length of 32 mm and was clamped onto the serrated faced grips. The extensometer of 25 mm length was fitted onto the specimen to record changes in length of the specimen. Upward constant speed of 3 mm/min on crosshead was applied. Destructive tensile test was conducted on all specimens.

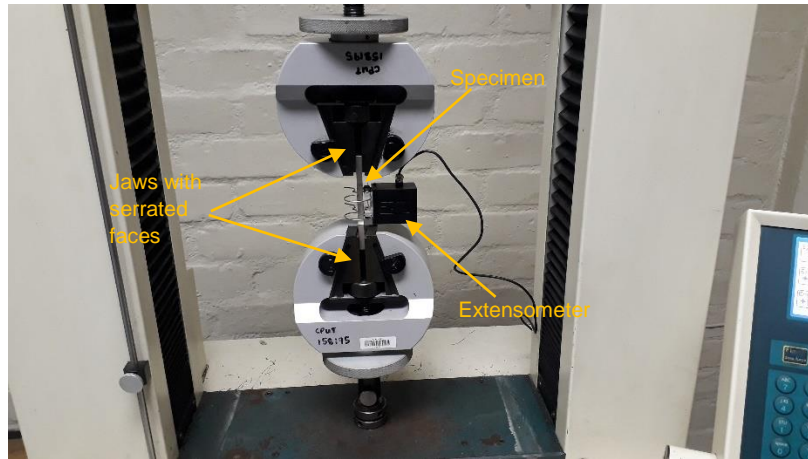


Figure 3.20: Tensile test set-up on Hounsfield Tinius Olsen H50KS

Figure 3.21 below is the tensile test specimens sampled from the start, middle and end of the weld respectively. Specimens were cut using electrical discharge machine (EDM) 0.25 wire in accordance with ASTM E8M-04.



Figure 3.21: Specimens for tensile testing

3.8.2 Bending testing

A Hounsfield Tinius Olsen on figure 3.22 was set on 1 mm/min speed in 3-point bending mode to achieve 90° bend on friction stir welded joints. Parent materials were set for 180° bend. All specimens were marked on the centre for easy allocation before and after the test.

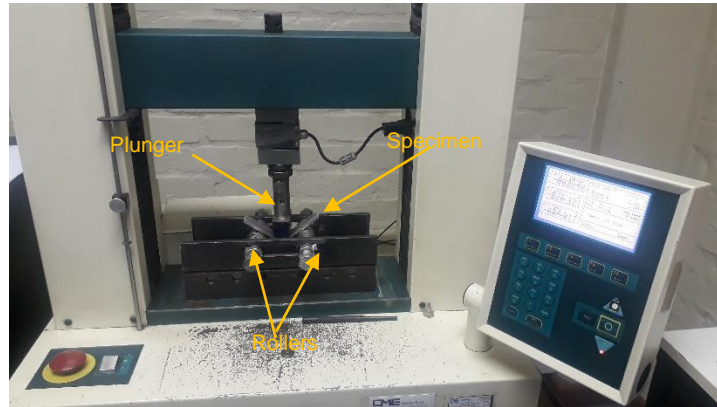


Figure 3.22: Bending test set-up on Hounsfield Tinius Olsen H50KS

Specimens were observed before testing for cracks along the edges and dents. Edges were noted to be smooth and the specimen did not show any prior unintended bending and free of scratches. On Figure 3.23, are the specimens prepared for bending test.

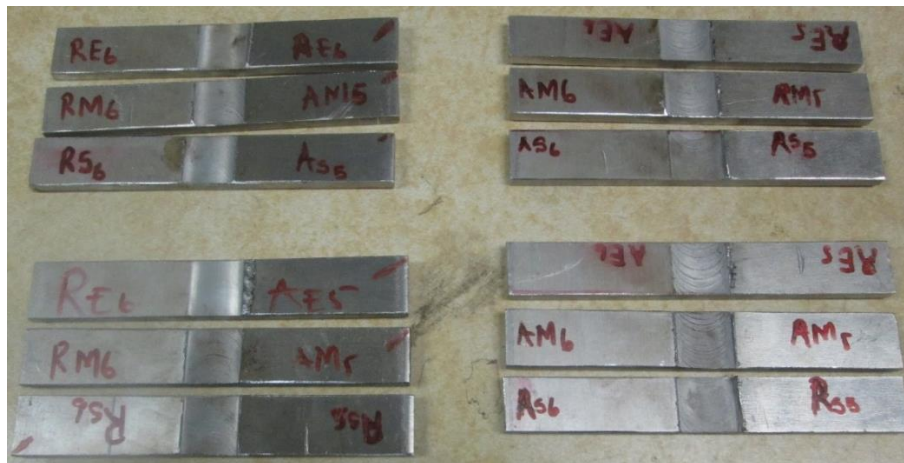


Figure 3.23: Bending specimens of welded joints

3.8.3 Liquid Penetrant Testing (LPT)

Non Destructive Testing (NDT) was conducted on the bent specimens to reveal possible defects on the surfaces. This was necessary to verify if indeed there were cracks developed after 90° and 180° bends. Figure 3.24 (a-c) demonstrate steps taken during LPT. In figure 3.24a, surfaces were thoroughly cleaned using Ardrex 9PR5 Aerosol solvent cleaner with the aid of non-fluffy cloth. Surfaces were allowed to dry

for three minutes. In figure 3.24b, Flaw Detector Penetrant 2 was applied and dwell time of eight minutes was observed. Ardrex 9PR5 Aerosol was applied on the cloth to remove flaw detector 2 penetrant. In figure 3.24c Ardrex 9D1B Developer was applied on the surfaces to allow capillary action. Developer was cleaned to reveal flaws.

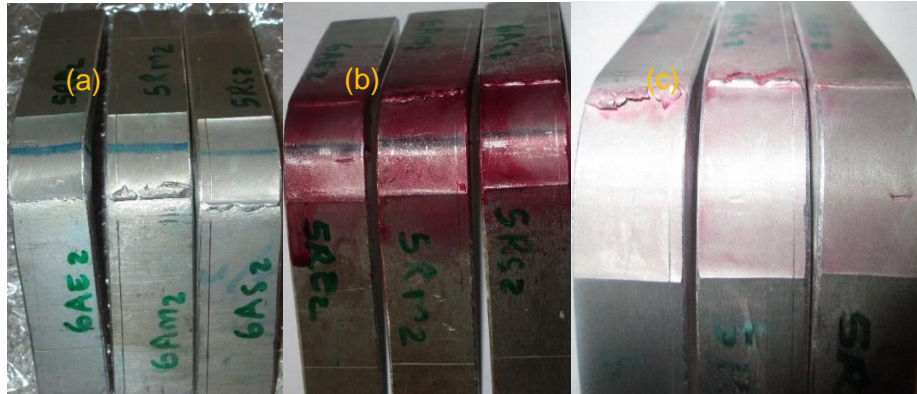


Figure 3.24 (a-c): Liquid penetrant applied on face weld joints

3.8.4 Micro-hardness

A micro-hardness profile was performed on the FSW welded samples for 5083-H321 on the advancing and also when it was on the retreating side. The testing was done through the cross section of the samples using a standard Vickers micro-hardness machine perpendicular to the welding direction at 6mm from the root face with a 300 gf applied for 10s. The indentations were spaced apart as shown on figure 3.25 (black dots) and a total length of 24 mm was covered. This was done to generate a hardness profile over the whole specimen. ASTM E 384 - standard test method for micro-hardness of materials was used in performing this test. Hardness traverse was done on the lateral side of the specimen to expose the depth of the weld rather than the face or the root of the joint as shown in figure 3.25.

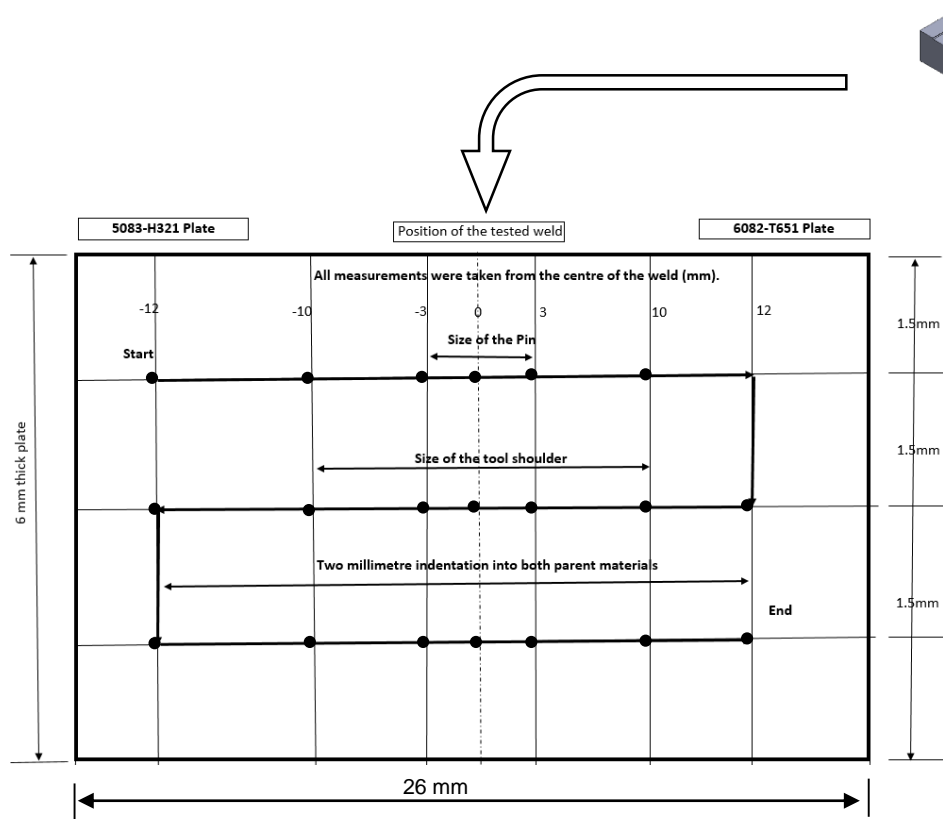


Figure 3.25: Hardness traverse profile of cross section

3.8.5 Metallographic tests

Metallographic tests were carried out to reveal macrographic post-weld regions/zones and micrographic test were done to transitions of grains from parent materials across the weld joint to another parent material. Grain sizes were also determined.

3.8.5.1 Macrostructure and microstructure tests

Metallurgical inverted AE2000 MET microscope was used to carry out micro and macro structural analysis to reveal surface flaws and to identify post weld zone of the weld joints. Polished and etched specimens were placed on the stage upside down as shown in figure 3.26. For macrostructure analysis, a 100X objective was used to view the structures. After focusing and adjustments 1000 microns picture was captured for analysis. For microstructure analysis, a 50X objective was used to view the microstructures. After focusing and adjustments 50 microns, the picture was captured for analysis.

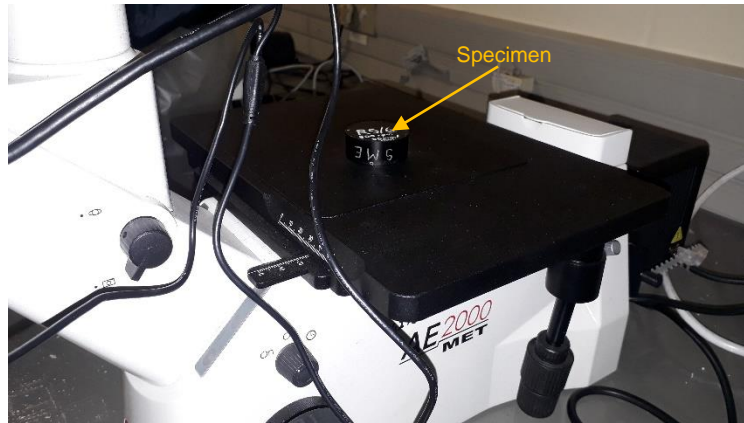


Figure 3.26: Macrostructure set-up on Hounsfield Tinius Olsen H50KS

3.8.6 Fractography by Scanning Electron Microscope (SEM)

Specimens were prepared for transgranular and intergranular analysis to check the nature of fracture and micro voids. Specimens for SEM were cut from middle specimens of tensile tests as indicated on figure 3.19. Specimens were cut such that the broken surface to be analysed were to be perpendicular to the SEM beam for best results. Hacksaw was used to cut specimens to a height of 5 mm. Cut surfaces were sanded parallel to the area to be analysed. Polishing disc was used to flatten the cut surfaces so that specimens were able to stand vertically. Copper double sided tape was cut using scissor. Copper double sided tape was then put on the stubs using a tweezer. Copper double sided tape served as conductor between specimens and stubs as shown on figure 3.27a. Firm pressure was applied to secure cut pieces on the stubs. All specimens were mounted on the stubs onto a pore-plate and secure using setscrews as shown on figure 3.27b.

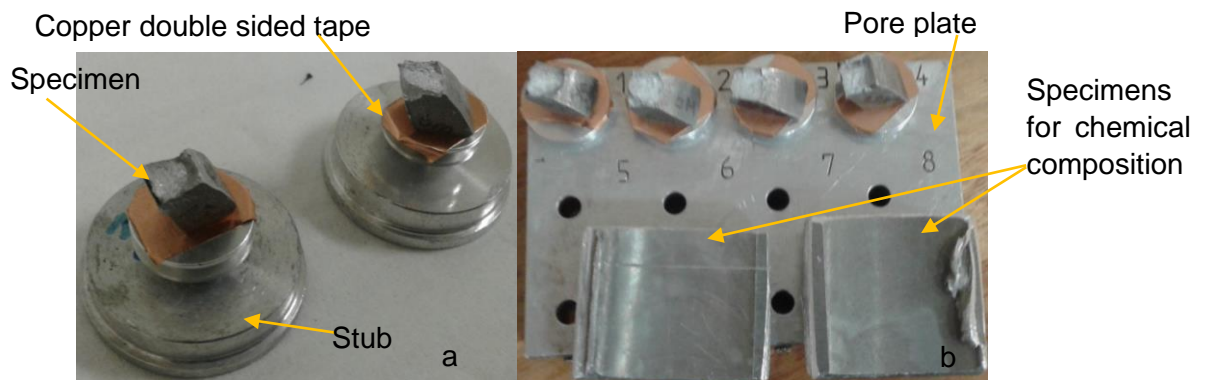


Figure 3.27: Specimens ready for loading into SEM

Chapter Four: Results and discussions

4.1 Friction Stir Welded joints chemical compositions

Parent materials together with welded joints were chemically tested to ascertain the chemical compositions. Table 4.1 presents chemical composition of parent materials, joints when both the 5083-H321 and 6082-T651 were advancing. Table 1(first two rows) is merged with table 4.1 for easy of comparing chemical compositions from literature and SEM measured results. The data in the first two rows was extracted from literature while the data in the last four rows was measured. As explained by [Davis, 2001] that 5083-H321 belongs to Al-Mg alloy with a prominence of manganese as a modification. On the other hand, the 6082-T651 is Al-Mg-Si alloy with addition of copper as a modification. FS welded joints when 5083-H321 advancing has a silicon below the minimum amount of 0.27% below 0.4%. Joint 6082-T651 on advancing side showed silicon within expectant range. Manganese on 5083-H321 is within reasonable level with the exception of 5083-H321 when advancing. The amount of magnesium for all parent material and FS welded joints was below the minimum except for 6082-T651 PM compare to literature. Copper showed unrealistic amounts compared to literature. The presence of aluminium on the parent materials was similar while 5083-H321 showed minimum aluminium content.

Table 4.1: Chemical composition of parent materials and welded joints

Alloy	Si	Fe	Mn	Mg	Cu	Cr	Al	O	Others
5083-H321 (from literature)	0.40	0.40	0.40- 1.0	4.0- 4.9	0.25	0.25	92	-	
6082-T651 (from literature)	0.7- 1.3	0.50	0.40- 1.0	0.6- 1.2	0.25	0.25	95	-	
5083-H321 (Wt %) (measured)	0.67	0.26	0.4	0.56	17.8	4.64	66.71	8.9	0
6082-T651 (Wt %) (measured)	-	0.24	0.44	4.6	18.1 3	-	65.05	11.54	0
Welded Joint (Wt %) 5 AS (measured)	0.27	0.43	0.32	2.55	30.9	-	58.17	7.28	0
Welded Joint (Wt %) 6 AS (measured)	1.07	1.35	0.66	3.23	-	-	80.77	10.63	2.29

4.1.1 Inspections of welded joints

All sheets were visually inspected after welding. Qualitative inspection of the welds was performed by visual inspection to detect surface defects, followed by metallographic analysis to detect internal flaws. Remarkable results can be obtained

by visual inspection to ascertain the possibility of macroscopic external defects, such as lack of penetration/surface-open tunnels, surface irregularities and excessive flashes.

4.1.1.1 Joint visual inspections

The inspection three basic types of defects: excessive flash, surface flaws (and internal voids figure 4.1(a) is a face weld when 5083-H321 was on advancing side, figure 4.1 (b) was face weld when 6082-T651 on the advancing side, figure 4.1 (c) is a root weld when 6082-T651 advancing, figure 4.1 (d) is root weld when 5083-H321 advancing and figure 4.1 (e-f) is the side view of the welds. Plates were all welded at 800 rpm and 60 mm/min speeds. Numerous authors that have been reviewed such as [Chandru et al., 2017, Sashank et al., 2018, Valate et al., (2016), Marhoon et al.,(2018), Jaiswal et al., (2014) and Kasman, 2013 to mention the few] had used range of tool rotational and traverse speeds and they found best results on 800 rpm and 60mm/min.

The surface appearance of weld joint when 5083-H321 (figure 4.1a) was on advancing side exhibited a smooth surface, smooth faded ripples and continuous flashes on the 5083-H321 alloy side. This was evident along the weld (from start to end of the weld joint) which can be attributed to:

- 1) Thirty second dwell time which allowed more heat generation.
- 2) The harder material (being 5083-T651) was placed on the advancing side which corroborates with literature [Rajani et al., 2012 and Uzun et al., 2005.] where sound welds were achieved when harder materials were placed on the advancing side.



Figure 4.1: Friction Stir Welded plates

Continuous flashes demonstrate ductility of the material and plastic deformation of the material experienced under the tool shoulder. The face welds on figure 4.1a exhibited smooth surface and its root weld figure 4.1d showed minimal roughness appearance.

In figure 4.1 (c and d), root welds are fully closed, deposited with plasticised material which gives indication that the tool has fully penetrated the plate thickness. It is reassuring also that on figures 4.1 (e and f) joint side views had no visible external macroscopic defects. This is the good indication that welding parameters were set properly. Smooth ripples are the evidence that heat input was enough for the tool shoulder to smoothen the surface, [Selamat et al., 2015].

A series of circular ripples with same pitch were evident when 6082-T651 (figure 4.1b) was on advancing side. Ripples appeared along the surface from start of the weld to end. It was observed that these ripples were essentially cycloidal and were produced by the final sweep of the trailing circumferential edge of the shoulder during traverse of the tool and this was in agreement with the findings of [Serio et al., (2016)]. The rotational speed of the tool and traverse speed of the work piece determines the pitch between the ripples. Root weld on figure 4.1c had a good smooth finish contrarily to the face weld. There were no macroscopic defects observed on joint side view on figure 4.1f which gives assurance of tool full penetration.

It is also worth noting that while there were continuous flashes for 5083-H321 on advancing side, while there were only circular ripples when 6082-T651 was advancing. When the tool rotates, it takes material from advancing side and sweeps it towards retreating side as it mixes [Kalemba-Rec et al., (2018)]. Due to harder material being placed on the retreating side, it did not plasticized enough to assist in smooth appearance of the joint surface. [Mehta, Kush P., 2019]

4.2 Metallographic analysis

4.2.1 Macro structural results and discussion

Figure 4.2 presents macrographic examinations which revealed post welding features for all the joints. Different post welded zones are shown to study the macrostructure of the welded sample. Figure 4.2 presents the welded joint consists of four different regions i.e. stir zone (SZ), thermo-mechanically affected zone (TMAZ), heat affected zone (HAZ) and parent material (PM).

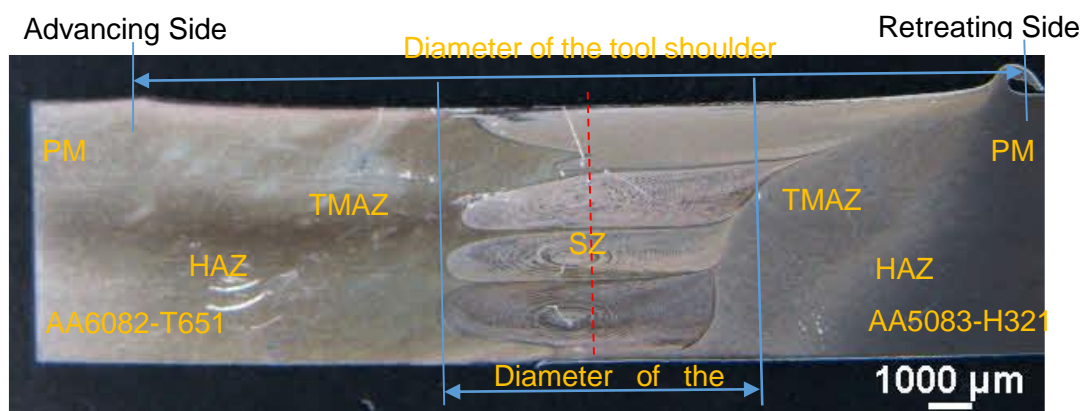


Figure 4.2: Post weld macrostructure.

It was observed on figure 4.2 that there was no distinct difference between HAZ and TMAZ on the 6082-T651 side, while the difference was clearly visible on the 5083-H321 side for advancing and retreating scenarios. The lateral flashes were evident on the 5083-H321 side only.

Three zones characterized the microstructure of the joint namely: stir zone (SZ), thermo-mechanically affected zone (TMAZ) and heat affected zone (HAZ). The joints are found to be defect free. TMAZ consisted deformed grains whereas the grains on the HAZ were not deformed during FSW though were subjected to a thermal heat cycle. SZ contains fine grains due to frictional heat and plastic deformation during friction stir welding [Tejonadha Babu et al., 2018]. The HAZ and TMAZ of the 6082-T651 were not clearly distinguishable as compared to that of 5083-H321.

Figure 4.3 (a-c) is 5083-H321 on advancing side while 6082-T651 in on retreating side. In figure 4.3, (a) is the start of the weld, (b) is the middle of the weld and (c) is the end of the weld. Figure 4.3 (d-f) is 6082-T651 on advancing side while 5083-H321 in on retreating side. In figure 4.3, (d) is the start of the weld, (e) is the middle of the weld and (f) is the end of the weld.

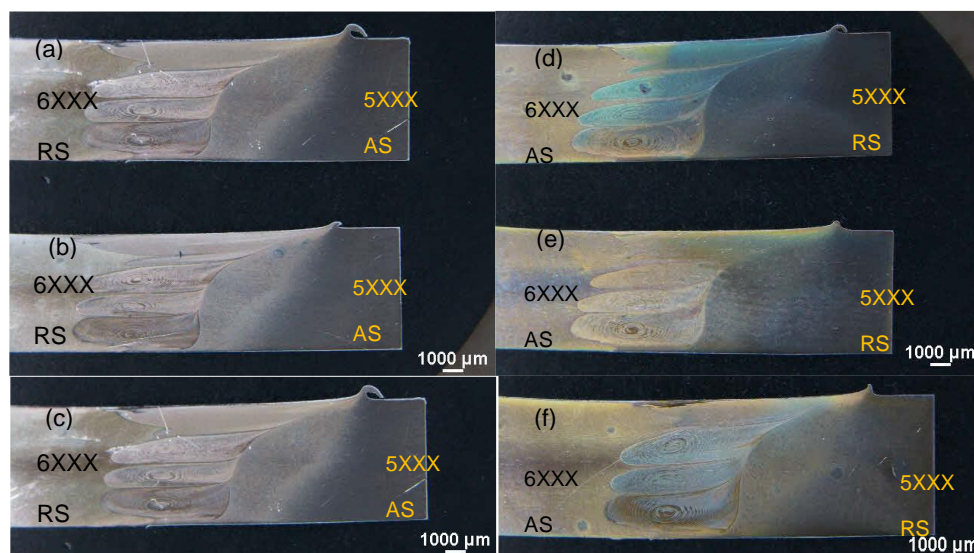


Figure 4.3: Macrostructure images (a-c) 5083 on AS and (d-f) 6082 on AS

All analyses revealed a good mixing and a good penetration of the tool in the joints. The results on figure 4.3 (a-e) are the confirmation of the visual inspection that the tool was fully inserted. There were no defects or irregularities observed. All macrographs presented nugget shapes with the typical “onion rings” that identified the mixing zone characteristic of FSW process. All macrostructures exhibited a regular post-weld features both retreating and advancing scenarios. It was observed that AA5083-H321 side on both scenarios exhibited a distinguishable TMAZ and good transition towards parent material. Stir zone was also noted having a well-defined boundary on the side of AA5083-H321, while on the side of AA6082 boundary takes the profile of the tool. It was particularly noted that, interfaces on the AA6082-T651 side for all the joints, appear to be serrated throughout the thickness of the plate. Dialami et al., (2019) explained

that these interfaces may be regarded to be an imperfection which is normally termed as “joint-line remnant” (JLR). Heat input enabled the material flow during the welding process. The JLR is mainly distributed on the boundary of stir zone SZ and (TMAZ) on retreating side (RS) of the welded joint [Besel et al., 2016]. This is partly in agreement with the results found in this study though the JLR is on both sides of the stir zone for advancing sides as well. It was observed that the microstructural mismatch exists between SZ, TMAZ and HAZ. The stir zones are also noted to be pointing towards the 5083-H321 side on advancing and retreating scenario. This contradicts the findings of [Khodir and Shibayanagi, 2007 and Çam and Mistikoglu, 2014] where the stir zones pointed towards the advancing sides only.

4.3 Microstructure analysis

Metallographic tests on the transverse cross sections of different welded samples were carried out to study the microstructure of different zones of the welded samples. Figure 4.4 presents microstructures for parent materials (PM). 5083-H321 had uniform grain sizes across the rolling direction (figure 4.4a). The grain size ranged from 18.50 µm along and 15.25 µm across the rolling directions. 6082-T651 had an average 20 µm along the rolling direction while achieving only 13 µm across the rolling direction.

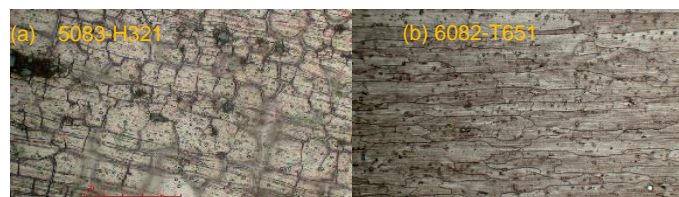


Figure 4.4: Parent material microstructures

It was observed that, in comparison to the PM microstructure (figure 4.4 and 4.5) showed considerable microstructural changes occurred after FSW, with the SZ consisting of equiaxed grains. It can be seen that the onion ring pattern well developed in centre of all the stir zones. With 5083-H321 on retreating side, smooth mixing can be seen from the start of the weld to the end of the weld. Materials are proportionally mixed, however towards the end of the weld, the intermixed particles 6082-H321 are becoming visible (R5S6, R5M6 & R5E6). Onion ring on the start of the weld (R5S6) had a rather homogeneous mixture of both materials while middle (R5M6) and end (R5E6) weld had an introduction of traces of magnesium and silicon on the onion rings.

With 5083-H321 on the advancing side, onion rings were characterized by visible magnesium and silicon traces. These magnesium and silicon traces are attributed to alloy 5083-H321 richness of these elements while 6082-T651 rich in silicon [Leitão et al., 2008]. The middle weld (A5M6) particularly had more concentration of magnesium and silicon traces. The stir zone with the 6082-T651 advancing has shown more homogeneity than when 5082-H321 advancing which has more intercalated layers of onion rings.

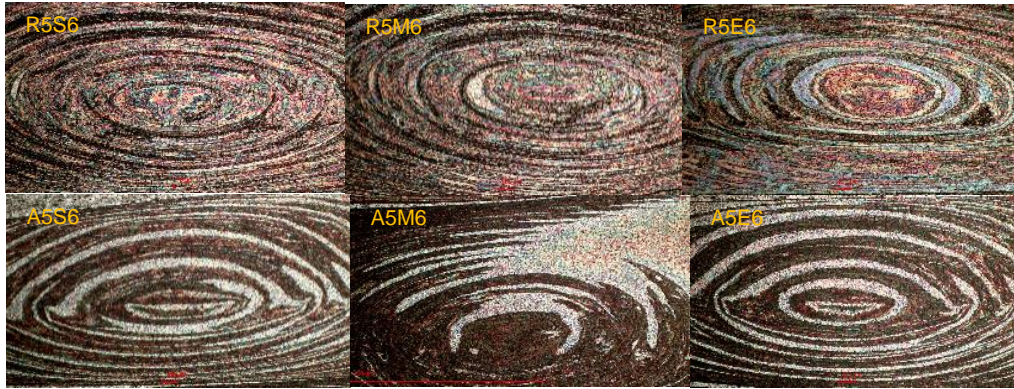


Figure 4.5: Stir zones of three samples for each scenario

Figure 4.6 presents average grain size pattern along the welded joint from the start of the weld to end of the weld joint for both scenario. The grain sizes of 5083-H321 when was on advancing side were smaller compared to when 6082-T651 was on advancing sides for all the joints. Graphs showed a mirror pattern where the middle welds had lowest values on 5083-H321 advancing while showed the highest value of grain size when the 6082-T651 advancing. Between the first and the last locations there was a slight difference recorded. The trend for grain size when 6082-T651 advancing decreased slightly as the distance increased while showed the slightly upward grain size trend when 5083-H321 advancing.

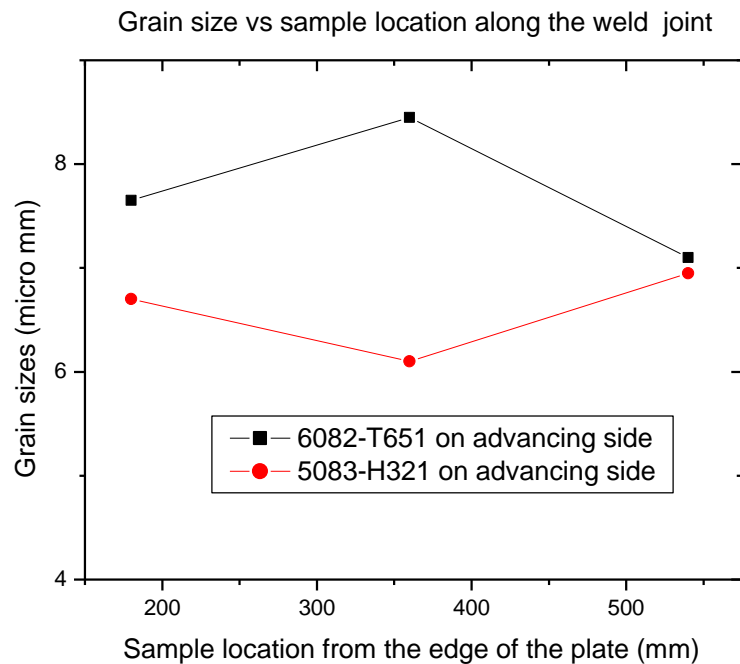
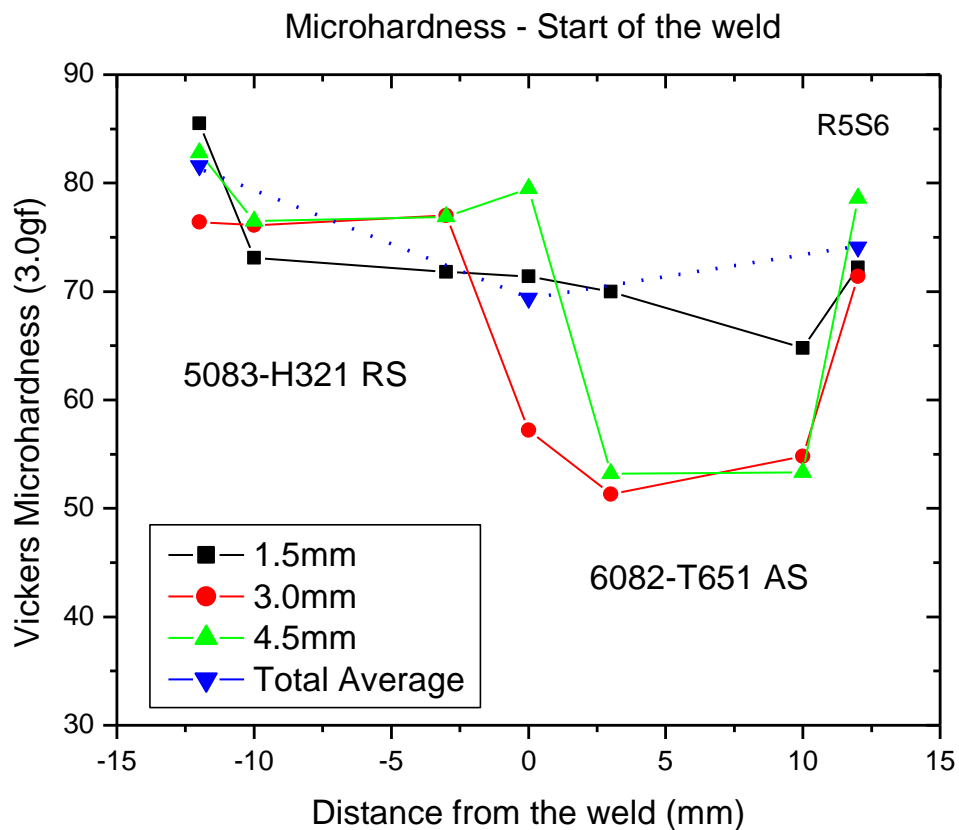


Figure 4.6: Grain size pattern for different conditions

4.4 Micro hardness analysis

The hardness distribution across the welded joints under different positions and depths is shown in figure 4.7. As expected 5xxx series shows greater hardness values than

the 6xxx series in all tests conducted. AA5083-H321 recorded an average of 85.0 HV which was also recorded in the study of Palani et al., (2018). The hardness values drop across all the welded joints towards AA6082-T651. The edges of the tool shoulder and tool pin positions on the AA5083-H321 reported minimal difference compared to the stir zones especially the start and middle weld positions while the end of the weld recorded higher values on the tool shoulder edges of the compared to the stir zone. Microhardness values at the 4.5 mm depth has the highest values in the stir zones for all positions while 3.0 mm depth shows least values. The edges of the tool pin and tool shoulder positions on the side of AA6082-T651 exhibited softness than all other positions. The total average hardness values in the stir zones from the start to the end positions of the weld joint showed an increase and even recorded more values than AA6082-T651 parent material. The increase in hardness in the stir zone is due to the fine grain size produced by FSW process and work hardened effect during the process [Hussein & Al-Shammari, (2018)].



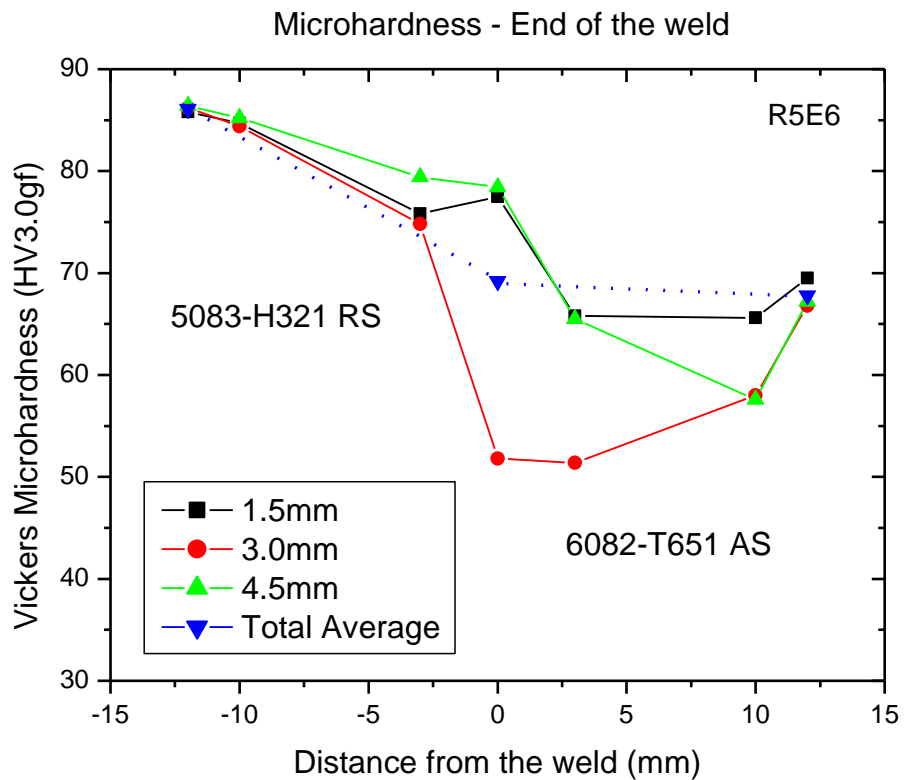
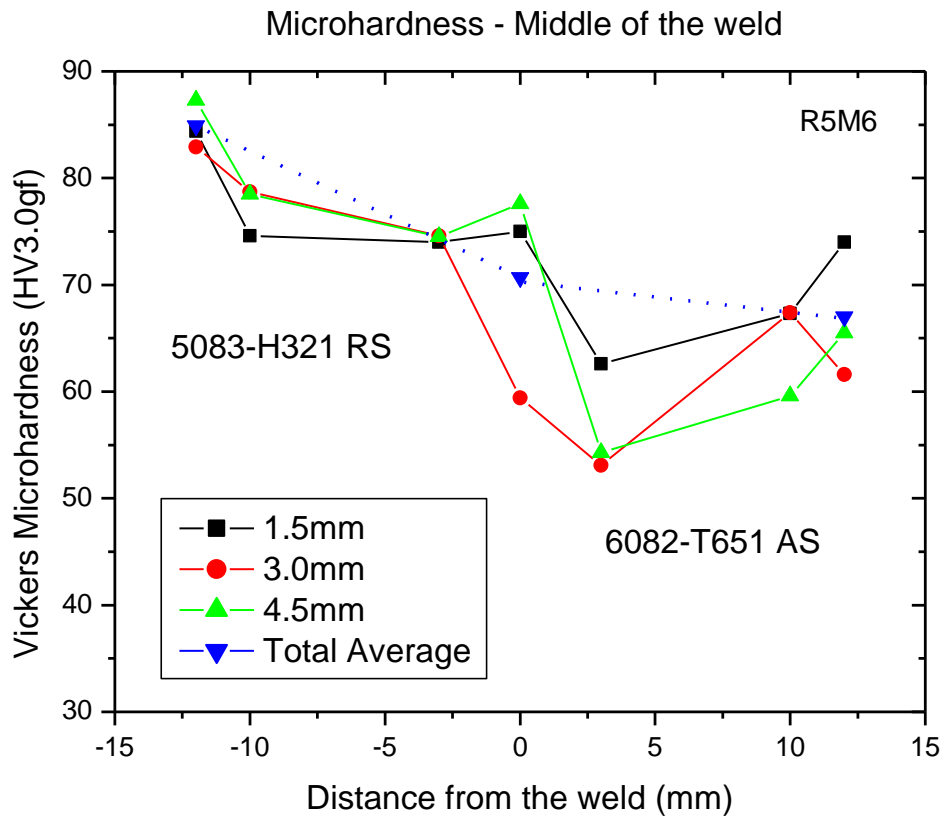
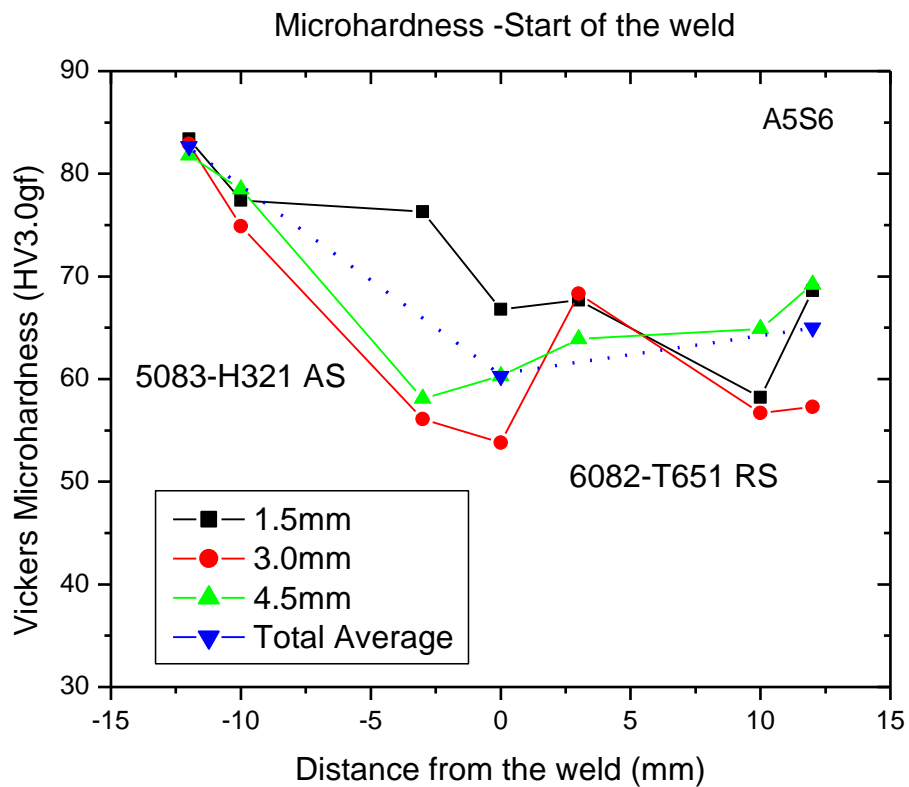


Figure 4.7: Microhardness profiles for R5S6, R5M6 and R5E6 of retreating AA5083-H321

Figure 4.8 presents results of microhardness with 5083-H321 on advancing side. Again with 5083-H321 on advancing side the hardness values are bigger than 6082-

T651 alloy when advancing. In the stir zone, the lowest hardness values of $\approx 55\text{HV}$ were recorded at 3.0 mm depth for all locations while 1.5mm exhibited higher values for all locations. The edges of the tool shoulder demonstrated less hardness values than tool pin positions on the 6082-T651. The stir zones proved to be softer than the soft base material contrary when the 6082-T651 is advancing. Microhardness values recorded average hardness value of less than 60HV compared to average of 70HV when 6082-T651 is retreating.

It was observed that, the 1.5 mm depth from the surface was characterised by high microhardness values on TMAZ of 5083-H321 for the start and middle weld except for the end of the weld position. 3.0 mm depth had high values for the start and middle weld also on the edge of the pin position except for the end of the weld position.



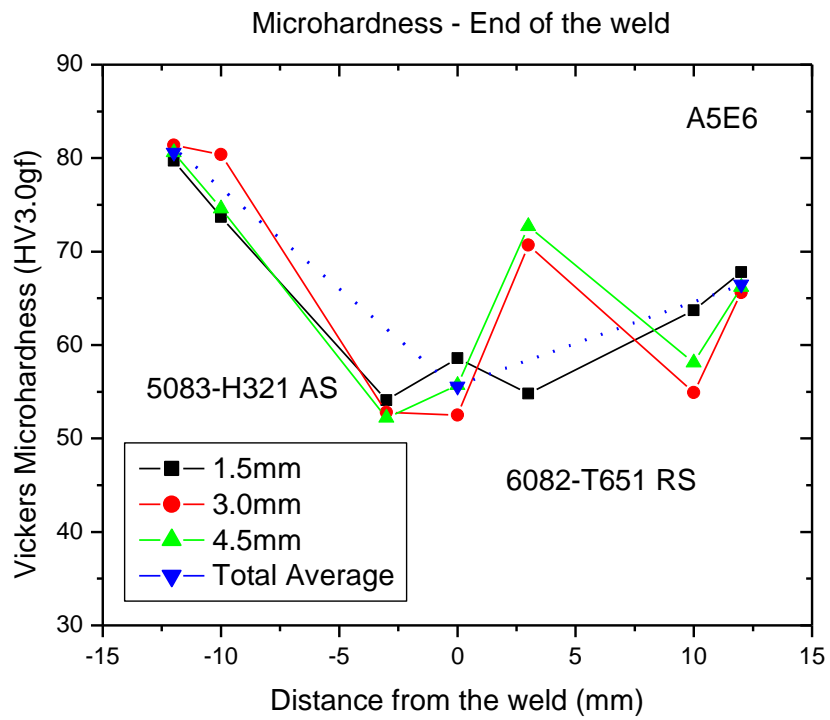
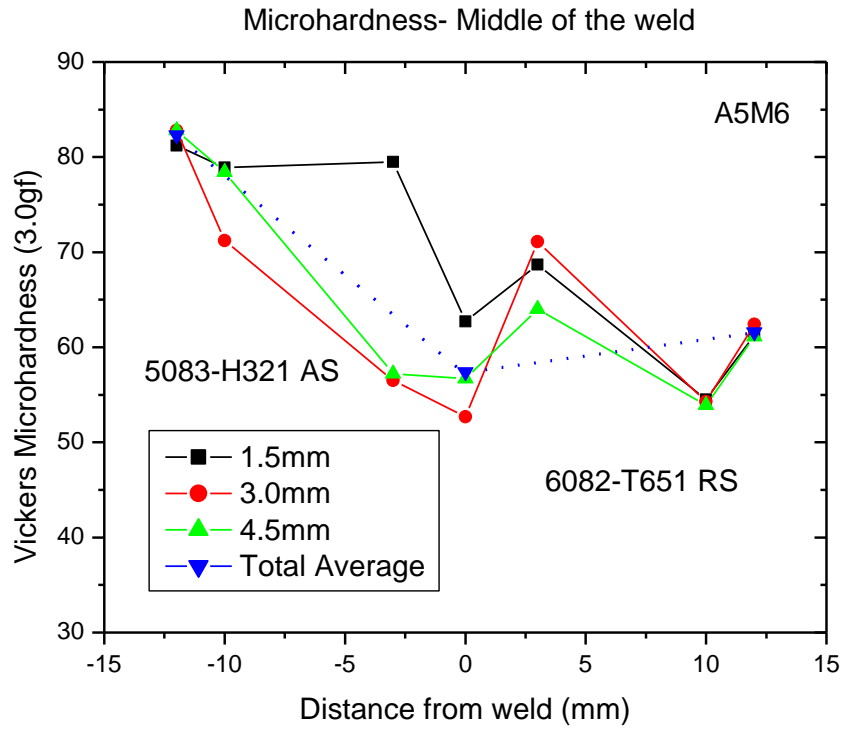


Figure 4.8: Microhardness profiles on different positions with AA5083-H321 on AS

4.5 Tensile test results of parent materials and FS welded joints.

Table 4.2: Traverse tensile properties of FSW joints

Joint type	Tensile Strength, σ_{UTS} (MPa)	Yield Strength, σ_y (MPa)	Elongation, (%)	Fracture location
5083-H321	317	228	16	CENTRE
6082-T651	290	250	10	CENTER
A5S6	187	155	7	HAZ/AA6082
A5M6	186	151	10	HAZ/AA6082
A5E6	188	156	9	HAZ/AA6082
R5S6	187	125	11	HAZ/AA6082
R5M6	181	135	9	HAZ/AA6082
R5E6	185	151	9	HAZ/AA6082

Figure 4.9 presents tensile tested specimens. When 5083-H321 was on the advancing side specimens broke on the end of the weld on the 6082-T651 side. Specimens broke on the 6082-T651 side also when 6082-T651 was advancing side. Necking was characterized by reduced area on the specimen. From Table 4, the % elongation range in the welded joint achieved was from 7-11%. As it can be seen, the higher average % elongation was found when 6082-T651 was on the advancing side. This is in-line with the results of stir zones where homogeneous mixture on 6082-T651 on advancing was found. Kumar et al., (2013) confirmed that the lower elongations are the results of coarse and non-homogeneous grain structures. This phenomenon is as a results of lower tool tilt angle and the large contact between tool shoulder and work-piece which produces excess heat and heat affected zone. It was observed that the stir zones when 5083-H321 was advancing were non-homogeneous.

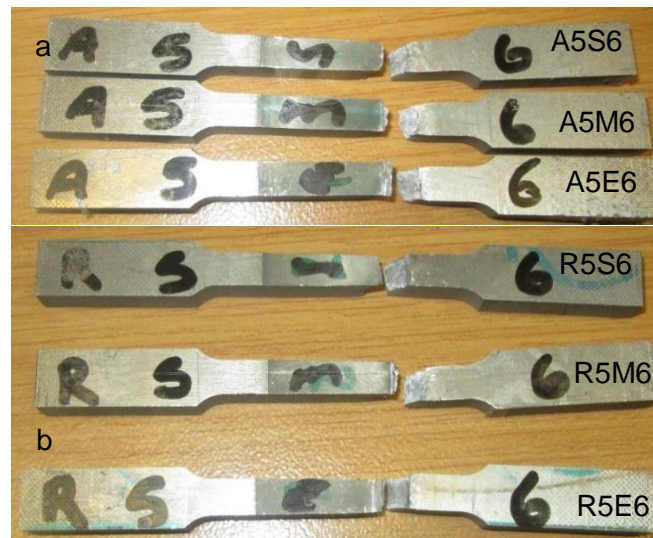
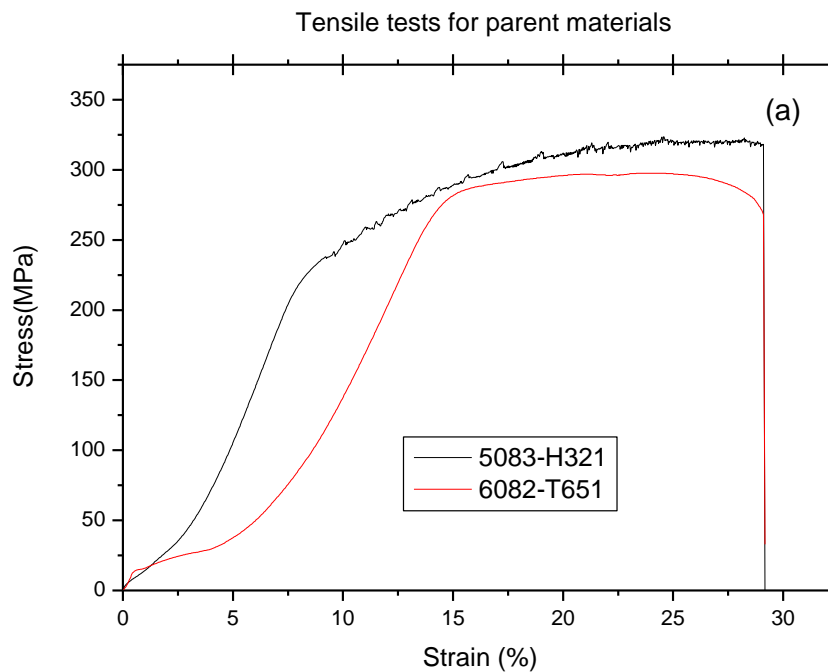


Figure 4.9(a-b): Visual examinations of two sets 5XXX advancing while 6XXX retreating and vice versa.

Figure 4.9 presents results of broken tensile specimen. All the welded joints were successfully broken under the applied load and speed. All specimens during tensile test failed at the edge of tool shoulder on the heat affected zone of the 6082-T651 side. This failure was observed in both conditions of retreating and advancing. Breaking points on the specimens correlate with microhardness graphs where they show that the softness was on the tool shoulder edges. The fact that the joint fractured outside the centre of the joint, in the HAZ meant that the joint is seamless [Sathari et al., 2015]. The fact that all specimens failed outside the joint gives a good indication that the joint is stronger than AA6082-T651. Liu et al., (2003) explained that the fracture sometimes occur at or near the interface between the stir zone and the TMAZ. This phenomenon is due to the difference in the internal structure of the stir zone and the TMAZ. The stir zone is characterised by fine-equiaxed recrystallized grains, while the TMAZ is characterised by coarse-twisted recovered grains. The interface between the stir zone and the TMAZ becomes the weaker area or position in the joint, and the joint is fractured at this interface during the tensile testing [Selamat et al., 2016].



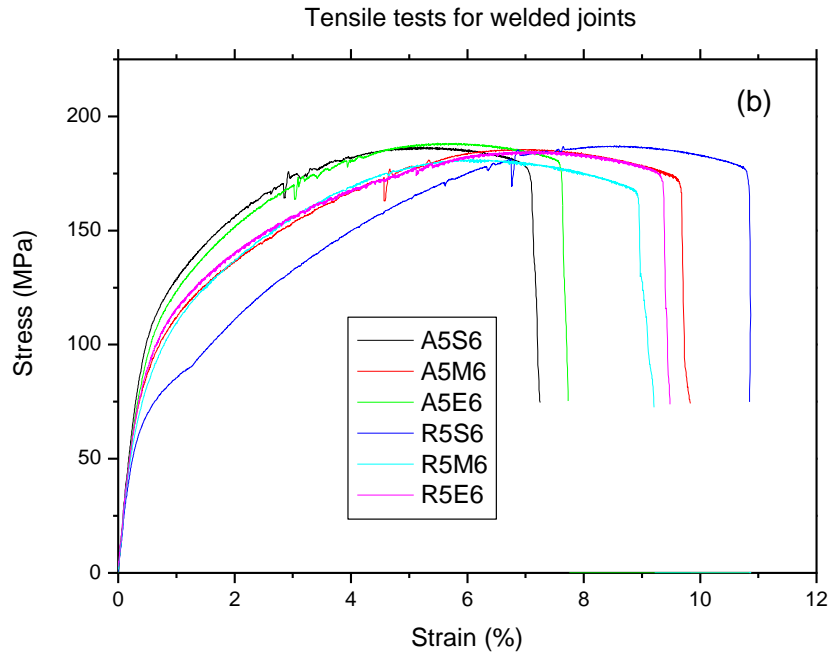


Figure 4.10 (a-b): Tensile test graphs for parent materials and Al-Alloys welded joints

Tensile stress-strain curves for the specimens obtained under different welding conditions are shown in Figure 4.10. The specimens obtained under the different welding conditions, the yield strength and ultimate strength during the tensile tests are ranging from 57-59% of 5083-H321 while 62-65% of the 6082-T651 base metals. With 5083-H321 advancing specimen achieve average of 187MPa and 184MPa on retreating. It was observed also that end of the weld specimen (A5E6) on 5083-H321 advancing achieved best UTS of 188MPa compared to middle specimen (R5M6) when 5083 retreating which obtained UTS of 181MPa. Both UTSs and yield for advancing and retreating showed similar pattern while the yield strength on 5083-H321 retreating showed steady increase of 21% from the start to the end of the weld location. It is worth noting that the specimen broke outside the joint interface which means that interface is stronger than 6082-T651. Parent materials achieved 28% strain while the joints ranged from 7 – 11% strain. The least being the start of the weld (A5S6) and the highest is start of the weld (R5S6) at 7% strain. When the 5083-H321 is advancing, the middle weld (A5M6) was the highest with 10% strain and the least is start of the weld (A5S6) at 7% strain. When the 6082-T651 is advancing, the start of the weld (R5S6) was the highest with 11% strain while the least was at the end of the weld (R5E6) at 8.5% strain. On average, the joint that achieved slight higher %strain is when 6082-T651 is advancing and also % strain decreased linearly from the start to the end of the weld on the same joint.

4.6 Bending test results of parent materials and FS welded joints

4.6.1 Bending specimen visual examinations and NDT on bent specimens.

Both parent material achieved 180° bend without visible cracks on the surfaces. Figure 4.11 shows bent specimen of parent material. It was noted that the bending was symmetrical as was expected of homogenous material. After the test it was observed that both parent materials achieved 180°. Surface of 5083-H321 was noted to be smooth while 6082-T651 had visible lumpiness texture on the surface. There were no defects noted on the edges of the bent plates.

Pictures for surface defects are taken on these top surfaces



Figure 4.11: Parent materials bent joints



Bend tests were carried out on all dissimilar specimen to determine the integrity of the welds by applying a uniform and constant load to the weld. Figure 4.12 shows bent specimens of welded joints. All the welded joints bent on the 6082-T651 side, which resulted in unsymmetrical bending. This is due to the difference in hardness of the two materials. 6082-T651 is a more malleable, softer alloy, therefore will deform more readily compared to the 5083-H321. 5083-H321 being the harder material shifted the effect of load onto 6082-T651 side. Welded joints achieved 90° bend. It can be observed that bending happened on the TMAZ and HAZ of the 6082-T651 for all the joints. This confirms the tensile tests specimen breaking points as the unsymmetrical bending was observed. It was found that all welded specimen passed the bend test of the dissimilar specimen which showed sufficient mixing.



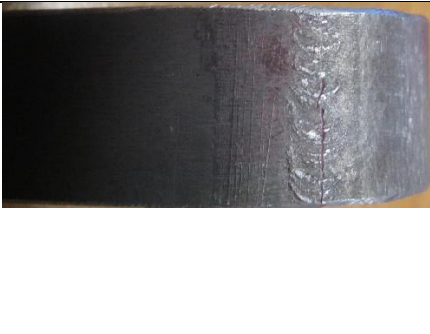
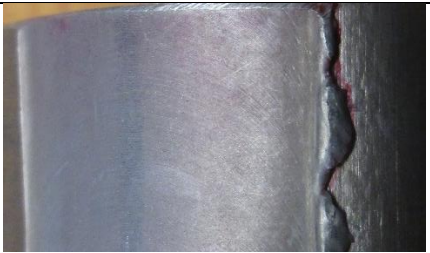








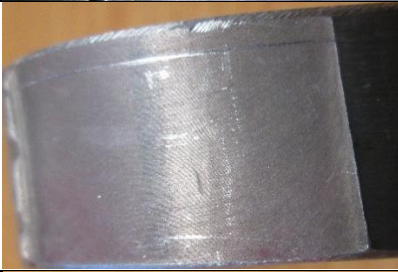

Figure 4.12: Bent dissimilar welded joints

Table 4.3 presents photographs of all the joints and defects found on each joint and possible reasons for the defect. Defects were mainly observed on the root welds. For the face welds, it was expected that cracks would propagate from the positions of the edges of the tool shoulder. This expectation was raised by tensile specimen breaking as they were all broken on the tool shoulder edges positions diagonally towards the weld interfaces.

Table 4.3: Analysis of the welded joints

Joint identification	Photographs of the bends	Defects and possible cause
5083-H321		Parent material 5083 had no defects observed. The surface appeared to be intact and smooth.
6082-T651		Parent material has lumpiness on the surface. Plastic deformation caused boundary grain dislocation.

<p>5AS1</p> <p>Root weld</p>		<p>Root weld has a crack where 5083 advancing on the start of the weld. Crack is attributed to thin layer which was not penetrated by the tool to avoid tool pin rubbing onto the back plate.</p>
<p>5AM1</p> <p>Root weld</p>		<p>Root weld has a crack where 5083 advancing on the middle of the weld. Crack is attributed to thin layer which was not penetrated by the tool to avoid tool pin rubbing onto the back plate.</p>
<p>5AE1</p> <p>Root weld</p>		<p>Root weld has a partial crack where 5083 advancing on the end of the weld. Crack is attributed to some portions of thin layer that was not penetrated by the tool. Rubbing of the tool pin on the back plate is observed by wavy patterns on the surface.</p>
<p>5AS2</p> <p>Face weld</p>		<p>Face weld joint has no visible for 5083 advancing at the start of the weld.</p>
<p>5AM2</p> <p>Face weld</p>		<p>Face weld joint has no visible for 5083 advancing at the middle of the weld.</p>
<p>5AE2</p> <p>Face weld</p>		<p>Face weld joint has a void for 5083 advancing at the end of the weld. Possible local foreign material under the surface along the interface during welding process.</p>

<p>5RS1</p> <p>Root weld</p>		<p>Root weld has a crack where 6082 advancing on the start of the weld. Crack is attributed to thin layer which was not penetrated by the tool to avoid tool pin rubbing onto the back plate.</p>
<p>5RM1</p> <p>Root weld</p>		<p>Root weld has a crack where 6082 advancing on the middle of the weld. Crack is attributed to thin layer which was not penetrated by the tool to avoid tool pin rubbing onto the back plate.</p>
<p>5RE1</p> <p>Root weld</p>		<p>Root weld has a crack where 6082 advancing on the end of the weld. Crack is attributed to thin layer which was not penetrated by the tool to avoid tool pin rubbing onto the back plate.</p>
<p>5RS2</p> <p>Face weld</p>		<p>Face weld no defect observed where 6082 advancing start of the weld.</p>
<p>5RM2</p> <p>Face weld</p>		<p>Face weld no defect on observed where 6082 advancing middle of the weld.</p>
<p>5RE2</p> <p>Face weld</p>		<p>Face weld no defect on observed where 6082 advancing end of the weld.</p>

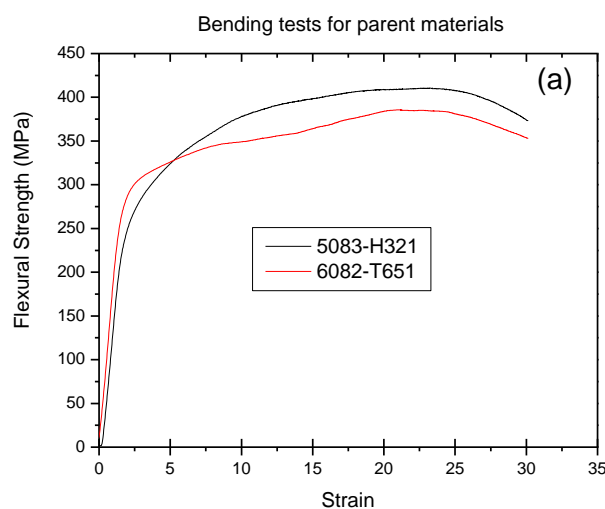
4.6.2 Bending test analysis of parent materials and FS welded materials

Figure 4.13 presents bending graphs for parent materials (a) and welded joints (b). Figure 4.13 (a) shows parent material, where 5083-H321 has achieved 384.84 MPa while 6082-T651 made 361.41MPa flexural strength. Flexural graphs for PM followed a pattern similar to that of tensile test graphs. It is also noted that bending strength is higher than that of tensile strength. This is because, in tensile test the entire cross sectional region undergoes tension stress while in bending test, the convex part of sample undergoes tension and the concave part undergoes compression.

Welded joint achieved flexural strength ranging from 199.69 MPa (5AM1 being the root middle weld 5083-H321 advancing) to 229.03 MPa (5AS2 being the face start weld 5083-H321 advancing) figure 4.13 (b). Root welding joints when 5083-H321 was advancing, ranged from 199.91MPa to 207.00 MPa, end weld being the highest while the middle weld showed least strength.

Face welding joints when 5083-H321 was advancing, ranged from 199.97 MPa to 229 MPa. The flexural strength pattern declined linearly from the start weld to the end weld. Root welding joints when 6082-T651 was advancing, ranged from 200.00 MPa to 225.28 MPa and the flexural strength pattern increased from the start weld to the end weld. Face welding joints when 6082-T651 was advancing, ranged from 207.00MPa to 223.88MPa, middle weld being the highest while the end weld was the least. Both face welds proved to be the stronger compared to the root welds where cracks were evident.

The elongations achieved by FSW joints are comparable closer to that of parent metals. The softer HAZ and TMAZ of 6082-T651 jointly contributed in total bending and hence the elongation is closer to that of parent materials though they were set for 90° bend than 180° bend of PM. Comparing tensile test and bending test graphs of the welded joints, it was noted that they shared a similar joint stiffness while with the parent materials, it was the bending graph that showed better stiffness. In figure 4.13 (b) graph is noted to have double ultimate flexural strengths. This is because two layers of the beam failed in separate stages as the beam experiences tension and compression during the bending test.



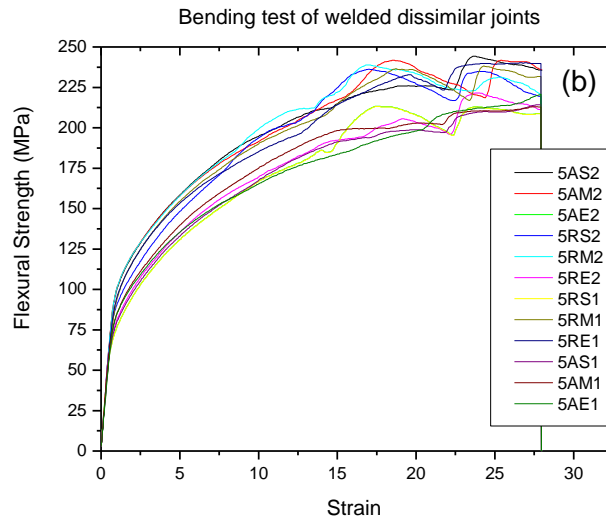


Figure 4.13: Graphical presentation of parent and welded joint materials

4.6.3 Liquid penetrant inspection (LPI)

Figure 4.14 presents surfaces after the (LPI) was removed. All joints after bending were tested for possible surface cracks using washable liquid penetrant. Figure 4.14 (a) is the PM 5083-H321, where there were neither cracks nor lumpiness on the surface observed. This confirms that the material after 180° bend did not crack. The 6082-T651 is presented on figure 4.14 (b). The surface was characterised by considerable lumpiness visible on the surface, however there was no capillary action observed on the surface. With the help of more advance NDT such ultrasonic testing or radiographic inspection subsurface flaws could be detected. Figure 4.14 (c) is one of the face weld where non showed signs of surface cracks except for the one suspected of surface impurities. LPI was only visible on the edges of the flashes. All the root bends (figure 4.14 d) were characterised by heavy ‘bleed-out’ of penetrant as indication of surface flaws. Flaws were identified to be the interface of the butt FSW joints which suffered partial penetration on the bottom surfaces during FSW process. This was also due to inconsistent applied force by the machine. It could be also due to flatness of the plate and the back-plate which get distorted by heat.

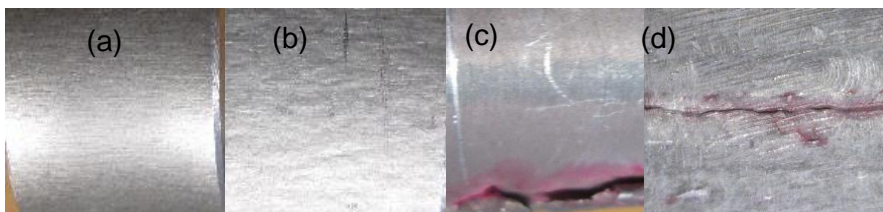


Figure 4.14: Surfaces after liquid penetrant solution

4.7 Scanning Electron microscope analysis

The tensile fracture morphology of the A5M6 welded joints are shown in Figure 4.15 (a-c). It can be seen that the fractures were full of circular dimples of different sizes with some deeper dimples in the HAZ/TMAZ of 6082-T651 advancing. It can be seen from the analysis results of the tensile specimen of the weld that the tensile fracture mode of the joint was a ductile fracture. The fracture on figure 4.15 (c) of the welded joint was mainly composed of small shallow equiaxial dimples. In figure 4.15 (b), the stress concentration reached the bonding strength between the Mg_2Si phase and the aluminium body. The Mg_2Si was separated from the interface of the body to form a microvoid, and the growth of the micro-void caused the internal necking of the specimen [Zhang & Wang, 2018].

The tensile fracture morphology of the R5M6 welded joints is shown in figure 4.15(d-f). Figure 4.15 (c-f) is from specimen R5M6 which is characterised by shear fractographs. This is the testimony to diagonal breaking of specimen from HAZ to TMAZ.

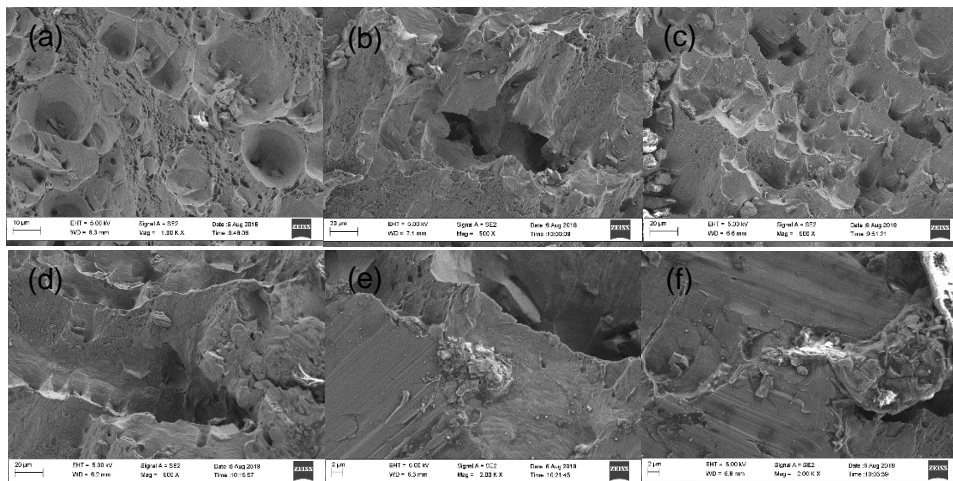


Figure 4.15: SEM macrographs

4.8 Summary

This section discussed some of the effect of defects on different test such as bending, tensile and microhardness. Bending specimens, bent in an asymmetrical manner, 6082-T651 being the soft alloys. This ties up with the breaking points on the tensile testing and confirmed by microhardness. During bending of root welds, it was revealed that the tool did not penetrate in some thin layers of plate. This, however did not promote the weakest point to be on the middle but it was found to be on the HAZ and TMAZ of 6082-T651. It seems that the edge of the tool cause more heat input on the 6082-T651 than 5083-H321. Aluminium alloy 6082-T651 as heat treatable alloys has no significant strengthening heat input of the tool shoulder. Aluminium alloy 5083-H321 on the other hand, as non-heat treatable alloy is subjected to a strain-hardening temper and in elevated temperature treatment for more stabilization than heat treatable alloys. This gives an advantage that non-heat treatable alloys are withstanding more heat than their counter parts.

Chapter Five: Conclusion and Future work

5.1 Conclusions

A literature review was conducted covering topics such as the friction stir welding process, tool geometry, tool materials, microstructure, and tensile strength and bending strength. Reasonable expectations of what to expect was then created through the literature review.

- Aluminium alloys 5083-H321 and 6082-T651 were successfully FS welded with the use of triflat threaded tool pin. There were continuous flashes for 5083-H321 on advancing side, while there were only circular ripples when 6082-T651 was advancing.
- In comparison to the PM microstructure, considerable microstructural changes occurred after FSW, with the SZ consisting of equiaxed grains. Grain sizes were refined on the stir zone compared to the PM, HAZ and TMAZ. 5083-H321 had uniform grain sizes across the rolling direction. Grain sizes when 5083-H321 advancing became smaller than when 6082-T651 advancing for all locations
- Different post weld zones were clearly visibly which supported the literature except for the 6082-T651 side where the TMAZ and HAZ of the 6082-T651 alloy not clearly distinguishable.
- For microhardness, with 5083-H321 on advancing side the hardness values were bigger than 6082-T651 alloy advancing.
- All specimens during tensile test failed at the edge of tool shoulder on the heat affected zone of the 6082-T651 side. With regards to % strain, the least was the start of the weld (A5S6) and the highest was start of the weld (A5S6) when 6082-T651 was advancing. When the 5083-H321 is advancing, the middle weld (A5M6) was the highest with 10% strain and the least is start of the weld (A5S6) at 7% strain. When the 6082-T651 is advancing, the start of the weld (R5S6) was the highest with 11% strain while the least was at the end of the weld (R5E6) at 8.5% strain.
- Parent materials bend up to 180° while welded joints managed 90°. All root welds cracked on the interface which is attributed to slight distortion of the plate and back-plate or maybe insufficient penetration. Face welded joint were superior to root weld. Liquid penetrant was used to verify the extent of cracks.
- Fractures were full of circular dimples of different sizes with some deeper dimples in the HAZ/TMAZ of 6082-T651 advancing.

Extraction of specimen from different locations did not affect results in any significant way. It was intermitted cases where it was found that from start to end weld results showed slight increase or decrease which could not definitely be attributed to the location as it did not happen consistently.

5.2 Future research

For future work, it appears that there is still room for improvement for the added features and accessories to our friction stir welding machine for more improved use.

The following can be done to improve the FSW machine:

- Thermocouples to measure the heat input along the weld joint.
- Loadcell to measure the plunge forces.
- Hall Effect sensors with LDTV.
- Change belt transmission to gear transmission for better torque during friction stir welding. This will assist in maintaining the position of the tool at or below the material surface.
- Use of hydraulic clamps for easy, quick and reliable clamping.
- Simulation software to experiment different materials such composite, polymers and compare experimental results with simulation for better understanding.

These features and accessories would also help to expand friction stir welding to other materials other than aluminium alloys.

The following studies need to be undertaken in FSW:

- The influence of breaking point position in FS welded tensile specimens.
- Guide to offset the tool during friction stir welding.

References

- A.Ramesh, Dr. M Indira Rani, A.P. 2016. Influence of tool design on the mechanical properties in friction stir welding of AA6082-T6 aluminum alloy. *Engineering Science and Technology, an International Journal*, 7(6): 5.
- Ahmed, M.M.Z., Ataya, S., El-Sayed Seleman, M.M., Ammar, H.R. & Ahmed, E. 2017. Friction stir welding of similar and dissimilar AA7075 and AA5083. *Journal of Materials Processing Technology*, 242: 77–91.
- Al-Jarrah, J.A., Ibrahim, M., Swalha, S., Gharaibeh, N.S., Al-Rashdan, M. & Al-Qahsi, D.A. 2014. Surface morphology and mechanical properties of aluminum-copper joints welded by friction stir welding. *Contemporary Engineering Sciences*, 7(January 2016): 219–230.
- Ambriz, R.R., Mayagoitia, V. & Ciitec-ipn, I.P.N. 2018. Welding of Aluminum Alloys. *Welding, Brazing and Soldering*, (i): 722–739.
- Asadi, M.K.B.G. and P. 2014. General introduction. In *Advances in Friction Stir Welding and Processing*. Elsevier Limited: 20.
- Çam, G. 2011. Friction stir welded structural materials: beyond Al-alloys. *International Materials Reviews*, 56(1): 1–48.
- Çam, G., Güçlüer, S., Çakan, A. & Serindag, H.T. 2009. Mechanical properties of friction stir butt-welded Al-5086 H32 plate. *Materialwissenschaft und Werkstofftechnik*, 40(8): 638–642.
- Çam, G. & Mistikoglu, S. 2014. Recent developments in friction stir welding of al-Alloys. *Journal of Materials Engineering and Performance*, 23(6): 1936–1953.
- Chandru, A., Ramesh, S. & Menon, P. 2017. Evaluation of Joint Properties of Aluminium Alloy After Friction Stir Welding. , (2015): 88–93.
- Dake, A.C.A. 2018. Chapter .1 Introduction. *In the spirit of the Red Banteng*: 1–5.
- Das, U. & Toppo, V. 2018. Bending Strength Evaluation of Friction Stir Welded AA6101-T6 and AA6351-T6 Aluminum Alloys Butt Joint. *Materials Today: Proceedings*, 5(5): 11556–11562. <https://doi.org/10.1016/j.matpr.2018.02.123>.
- Davis, J.R. 2001. Aluminum and Aluminum Alloys. *Light Metals and alloys*: 66.
- DebRoy, T. & Bhadeshia, H.K.D.H. 2010. Friction stir welding of dissimilar alloys – a perspective. *Science and Technology of Welding and Joining*, 15(4): 266–270. <http://www.tandfonline.com/doi/full/10.1179/174329310X12726496072400>.
- Devaiah, D., Kishore, K. & Laxminarayana, P. 2017. Effect of Welding Speed on Mechanical Properties of Dissimilar Friction Stir Welded AA5083-H321 and AA6061-T6 Aluminum Alloys. *International Journal of Advanced Engineering Research and Science*, 4(3): 22–28.
- El-Shennawy, M., Abdel-Aziz, K. & Omar, A.A. 2017. Metallurgical and mechanical properties of heat treatable aluminum alloy AA6082 welds. *International Journal of Applied Engineering Research*, 12(11): 2832–2839.
- Gordon, S. 2010. *Friction stir welding*.
- Gungor, B., Kaluc, E., Taban, E. & Sik, A. 2014. Mechanical, fatigue and microstructural properties of friction stir welded 5083-H111 and 6082-T651 aluminum alloys. *Materials*

and Design, 56: 84–90.

- Hasan, M.M., Ishak, M. & Rejab, M.R.M. 2016. A simplified design of clamping system and fixtures for friction stir welding of aluminium alloys. *Journal of Mechanical Engineering and Sciences*, 9(December): 1628–1639.
- Hussein, W. & Al-Shammari, M.A. 2018. Fatigue and Fracture Behaviours of FSW and FSP Joints of AA5083-H111 Aluminium Alloy. *IOP Conference Series: Materials Science and Engineering*, 454(1).
- Ibrahimmahoon, I., Al-Kamal, A.K. & Ali Abdulrehman, M. 2018. Studying the Mechanical Properties for 5086 Aluminum Alloy Welded Plates by Friction Stir Welding (FSW). *IOP Conference Series: Materials Science and Engineering*, 454(1).
- Jain, S., Sharma, N. & Gupta, R. 2017. Dissimilar alloys (AA6082/AA5083) joining by FSW and parametric optimization using Taguchi, grey relational and weight method. *Engineering Solid Mechanics*, (January): 51–66.
- Jaiswal, D., Kumar, R., Singh, R., Pandey, S. & Prasad, R. 2014. Influence of Cooling Media on Mechanical Properties of Friction Stir Welded 1060 Aluminium Alloy. , 10(4): 54–57.
- K. J. Colligan. 2010. The friction stir welding process: an overview. In D. L. and Z. Chen, ed. *Friction stir welding From basics to applications*. USA: Woodhead Publishing Limited: 15–28.
- Kalembe-Rec, I., Kopyściański, M., Miara, D. & Krasnowski, K. 2018. Effect of process parameters on mechanical properties of friction stir welded dissimilar 7075-T651 and 5083-H111 aluminum alloys. *International Journal of Advanced Manufacturing Technology*, 97(5–8): 2767–2779.
- Kamm, J. & Voort, G. Vander. 1939. Solutions for Materials Preparation, Testing and Analysis An Introduction to Microindentation Methods. , 1(6): 1–5. www.buehler.com.
- Kasman, Ş. 2013. Optimisation of dissimilar friction stir welding parameters with grey relational analysis. *Proceedings of the Institution of Mechanical Engineers, Part B: Journal of Engineering Manufacture*, 227(9): 1317–1324.
- Kasman, S., Kahraman, F., Emiralioğlu, A. & Kahraman, H. 2016. A Case Study for the Welding of Dissimilar EN AW 6082 and EN AW 5083 Aluminum Alloys by Friction Stir Welding. *Metals*, 7(1): 6.
- Kaur, M., Singh, T. & Singh, K. 2016. Comparison between Friction stir welding & Fusion welding of Aluminium Alloys based on mechanical properties & microstructure: *International Journal of Recent Advances in Engineering & Technology* 4(2): 2–5.
- Khodir, S.A. & Shibayanagi, T. 2007. Microstructure and Mechanical Properties of Friction Stir Welded Dissimilar Aluminum Joints of AA2024-T3 and AA7075-T6. *Materials Transactions*, 48(7): 1928–1937. <http://joi.jlc.jst.go.jp/JST.JSTAGE/matertrans/MRA2007042?from=CrossRef>.
- Krzysztof, M. & Kurtyka, P. 2015. Microstructure and properties of 6082 aluminium alloy friction stir welded with different parameters of welding MICROSTRUCTURE AND PROPERTIES OF 6082 ALUMINIUM ALLOY FRICTION STIR WELDED WITH DIFFERENT. , (January 2012).
- Kumar, N., Yuan, W. & Mishra, R.S. 2015. *Friction Stir Welding of Dissimilar Alloys and Materials*. <http://www.sciencedirect.com/science/article/pii/B9780128024188000011>.

- Kumar, Y., Kumar, A. & Rajyalakshmi. 2014. Optimization of process parameters during Friction Stir Welding of Aluminium 5083 & 6082 Alloys. , 4(6): 4144–4152.
- Leitão, C., Leal, R.M., Rodrigues, D.M., Vilaça, P. & Loureiro, A. 2008. Material flow in friction stir welding. *Microscopy and Microanalysis*, 14(SUPPL. 3): 87–90.
- Liu, F., Fu, L. & Chen, H. 2018. Microstructure Evolution and Mechanical Properties of High-Speed Friction Stir Welded Aluminum Alloy Thin Plate Joints. *Journal of Materials Engineering and Performance*, 27(7): 3590–3599.
- Liu, H.J., Fujii, H., Maeda, M. & Nogi, K. 2003. Tensile properties and fracture locations of friction-stir-welded joints of 2017-T351 aluminum alloy. *Journal of Materials Processing Technology*, 142(3): 692–696.
- Lohwasser, D. & Chen, Z. 2010. *Friction Stir Welding: From Basics to Applications*.
- Magee, R. V., سلامة م, Magee, R. V., Crowder, R., Winters, D.E., Beerbower, E., Bodhi, B., Schindler, S., Pfattheicher, S., Reinhard, M.-A., Haddock, G., Foad, C., Windsor-Shellard, B., Dummel, S., Adarves-Yorno, I., Furlotte, C. & Gorski, P.C. 2017. No Title الاجراءات ال اجنائة. *ABA Journal*, 102(4): 24–25. http://www.tandfonline.com/doi/abs/10.1080/14639947.2011.564813%0Ahttp://dx.doi.org/10.1080/15426432.2015.1080605%0Ahttps://doi.org/10.1080/15426432.2015.1080605%0Ahttp://heinonline.org/HOL/Page?handle=hein.journals/abaj102&div=144&start_page=26&collectio.
- Mehta, Kush P. (January 2019). "A review on friction-based joining of dissimilar aluminum–steel joints". *Journal of Materials Research*. 34: 78–96.
- Mishra, A. 2018a. Friction Stir Welding of Dissimilar Metal: A Review. *Ssm*, (January).
- Mishra, A. 2018b. Friction Stir Welding Of Dissimilar Metal: A Review Study on corrosion resistance of Friction stir welded similar joints of Aluminium alloy. View project MECHANICAL AND METALLURGICAL CHARACTERIZATION OF MAGNESIUM COMPOSITES THROUGH SQUEEZE CASTING View pr. , (January). <https://www.researchgate.net/publication/322551618>.
- Mishra, R.S. & Ma, Z.Y. 2005. Friction stir welding and processing. *Materials Science and Engineering R: Reports*, 50(1–2): 1–78.
- Mishra, R.S. & Mahoney, M.W. 2007. Friction Stir Welding and Processing. *ASM International*: 368.
- Moreira, P. & Jesus, A. 2008. Fatigue Crack Growth Behaviour of the Friction Stir Welded 6082-T6 Aluminium Alloy. *Revista da Associação ...*: 99–106.
- Moreira, P.M.G.P., Santos, T., Tavares, S.M.O., Richter-Trummer, V., Vilaça, P. & de Castro, P.M.S.T. 2009. Mechanical and metallurgical characterization of friction stir welding joints of AA6061-T6 with AA6082-T6. *Materials and Design*, 30(1): 180–187.
- Morishige, T., Kawaguchi, A., Tsujikawa, M., Hino, M., Hirata, T. & Higashi, K. 2008. Dissimilar Welding of Al and Mg Alloys by FSW. *Materials Transactions*, 49(5): 1129–1131.
- Nadim, A.A. & Ahmed, H. 2014. Design, Fabrication and Testing of Friction Stir Welded Joints. *International Journal of Innovative Research in Science, Engineering and Technology*, 03(11): 17261–17268.
- Navaneethkrishnan, T. & Ganesh, P. 2015. Effect of welding parameters on friction stir welded dissimilar aluminum alloys 7075 and 6082 with various tool pin profiles. *Journal of Chemical and Pharmaceutical Sciences*, 2015-April(9): 463–468.

- Nur, R., Sultan, A.Z. & Suyuti, M.A. 2017. Mechanical properties on friction stir welding of aluminum alloy 5052. *ARPN Journal of Engineering and Applied Sciences*, 12(15): 4445–4450.
- Olabode, M., Kah, P. & Martikainen, J. 2013. Aluminium alloys welding processes: Challenges, joint types and process selection. *Proceedings of the Institution of Mechanical Engineers, Part B: Journal of Engineering Manufacture*, 227(8): 1129–1137.
- Palani, K., Elanchezian, C., Saiprakash, K.H.V., Sreekanth, K., Dayanand, D., Kumar, K. & Kumar, D. 2018. Effect of welding parameters on mechanical properties of dissimilar Friction Stir Processed AA 8011 and AA 5083-H321 aluminium alloys. *IOP Conference Series: Materials Science and Engineering*, 390(1).
- Palanivel, R., Koshy Mathews, P., Dinaharan, I. & Murugan, N. 2014. Mechanical and metallurgical properties of dissimilar friction stir welded AA5083-H111 and AA6351-T6 aluminum alloys. *Transactions of Nonferrous Metals Society of China (English Edition)*, 24(1): 58–65. [http://dx.doi.org/10.1016/S1003-6326\(14\)63028-4](http://dx.doi.org/10.1016/S1003-6326(14)63028-4).
- Pantelis, D.I. 2014. Greek Section, Technical Meeting. , (May): 1–57. https://higherlogicdownload.s3.amazonaws.com/SNAME/e10ad46f-35fe-4b7d-a4cf-3da678bacc3f/UploadedImages/Pantelis_SNAME_in_english_v1.pdf.
- Parida, B., Vishwakarma, S.D. & Pal, S. 2015. Design and development of fixture and force measuring system for friction stir welding process using strain gauges. *Journal of Mechanical Science and Technology*, 29(2): 739–749.
- Patel, V., Li, W., Wang, G., Wang, F., Vairis, A. & Niu, P. 2019. Friction Stir Welding of Dissimilar Aluminum Alloy Combinations: State-of-the-Art. *Metals*, 9(3): 270.
- Patil, H.S. & Soman, S.N. 2014. Effect of tool geometry and welding speed on mechanical properties and microstructure of friction stir welded joints of Aluminium alloys AA6082-T6. *Archive of Mechanical Engineering*, 61(3): 455–468.
- Ranjith R & Kumar SB., 2014. Joining of dissimilar aluminium alloys AA2014 T651 and AA6063 T651 by friction stir welding process. *Wseas Transactions On Applied And Theoretical Mechanics* (unpublished).
- Ravindar, B. & Gururaj, K. 2015. Effects of Friction Stir Welding Parameters on Butt Joint Properties of Aluminium Alloy 5083. *Internastional journal of innovative research in science, engineering and technology*, 4(7): 6531–6537.
- Sangalli, G., Vieira, G., Lemos, B., Martinazzi, D., Lessa, L., Beskow, A.B. & Reguly, A. 2019. Towards Qualification of Friction Stir Welding to AA5083-O and AA5052-O Aluminum Alloys. , 22(5): 1–8.
- Saravanakumar, R., Krishna, K., Rajasekaran, T. & Siranjeevi, S. 2018. Investigations on friction stir welding of AA5083-H32 marine grade aluminium alloy by the effect of varying the process parameters. *IOP Conference Series: Materials Science and Engineering*, 402(1).
- Sarsilmaz, F. 2017. Relationship between microstructure and mechanical properties of dissimilar aluminum alloy plates by friction stir welding Furkan Sarsilmaz 1* 1. : 1–12.
- Sashank, J.S., Sampath, P., Krishna, P.S., Sagar, R., Venukumar, S. & Muthukumar, S. 2018. Effects of friction stir welding on microstructure and mechanical properties of 6063 aluminium alloy. *Materials Today: Proceedings*, 5(2): 8348–8353. <http://linkinghub.elsevier.com/retrieve/pii/S2214785317327979>.
- Sathari, N.A.A., Razali, A.R., Ishak, M. & Shah, L.H. 2015. Mechanical strength of dissimilar

- AA7075 and AA6061 aluminum alloys using friction stir welding. *International Journal of Automotive and Mechanical Engineering*, 11(1): 2713–2721.
- Selamat, N.F.M., Baghdadi, A.H., Sajuri, Z. & Kokabi, A.H. 2016. Friction stir welding of similar and dissimilar aluminium alloys for automotive applications. *International Journal of Automotive and Mechanical Engineering*, 13(2): 3401–3412.
- Selamat, N.F.M., Baghdadi, A.H., Sajuri, Z. & Kokabi, A.H. 2015. Friction stir welding of similar and dissimilar Aluminium alloys joining for Automotive. *International conference on recent advances in automotive engineering & mobility research*: 1-3 December.
- Serio, L.M., Palumbo, D., Alberto, L., Filippis, C. De, Galietti, U. & Ludovico, A.D. 2016. Effect of Friction Stir Process Parameters on the Mechanical and Thermal Behavior of 5754-H111 Aluminum Plates. *Materials*, 122: 1–19.
- Shanmuga Sundaram, N. & Murugan, N. 2010. Tensile behavior of dissimilar friction stir welded joints of aluminium alloys. *Materials and Design*, 31(9): 4184–4193. <http://dx.doi.org/10.1016/j.matdes.2010.04.035>.
- Shigematsu, I., Kwon, Y.J., Suzuki, K., Imai, T. & Saito, N. 2003. Joining of 5083 and 6061 aluminum alloys by friction stir welding. *Journal of Materials Science Letters*, 22(5): 353–356.
- Shiva Chander, M., Satish Kumar, P. & Devaraju, A. 2018. Influence of Tool Rotational speed and Pin Profile on Mechanical and Microstructural Characterization of Friction Stir Welded 5083 Aluminium Alloy. *Materials Today: Proceedings*, 5(2): 3518–3523. <https://doi.org/10.1016/j.matpr.2017.11.599>.
- Singh, K., Singh, G. & Singh, H. 2018. Review on friction stir welding of magnesium alloys. *Journal of Magnesium and Alloys*, 6(4): 399–416. <https://doi.org/10.1016/j.jma.2018.06.001>.
- Śliwa, R.E., Myśliwiec, P., Ostrowski, R. & Bujny, M. 2019. Possibilities of joining different metallic parts of structure using friction stir welding methods. *Procedia Manufacturing*, 27: 158–165.
- Soeripto. 1998. Ergonomi dan Produktivitas Kerja. *Makalah Hiperkes dan KK*, 90712(July).
- Sravanthi, C. 2016. Analogizing of Convention Fusion Welding Processes with Solid-State Welding Technique. , 3(04): 14–18.
- Srinivasulu, P., Rao, G.K.M. & Gupta, M.S. 2015. Evaluation of Bending Strength of Friction Stir Welded Aa 6082 Aluminum Alloy Butt Joints. , 8354(4): 1262–1270.
- Tejonadha Babu, K., Muthukumar, S. & Bharat Kumar, C.H. 2018. A study on grain size, mechanical properties and first mode of metal transfer in underwater friction stir welded AA5052-O. *Key Engineering Materials*, 775 KEM(August): 466–472.
- Thomas, W.M.W., Norris, I., Nicholas, E.D., Needham, J.C., Murch, M.G., Temple-Smith, P. & Dawes, C.J. 1991. Friction stir welding process developments and variant techniques. *Google patents*, (January 2005): 1–21. <http://www.google.com/patents/US5460317%5Cn>.
- Uzun, Huseyin; Dalle Donne, Claudio; Argagnotto, Alberto; Ghidini, Tommas; Gambaro, Carla (February 2005). "Friction stir welding of dissimilar Al 6013-T4 To X5CrNi18-10 stainless steel". *Materials & Design*. 26 (1): 41–46.
- V.Sivaramakrishna, S.N. 2015. Experimental Investigation of Friction Stir Welding and TIG Welding for Al-6082. *International Journal of Innovative Research in Science*,

Engineering and Technology, 04(07): 5292–5298.

Valate, A., Raut, A., Salunke, S., Thombare, S. & Umbarkar, A.M. 2016. Investigation of Variation in Tensile Strength of FSW Butt joints of Al 6082-T6 aluminum with Welding Speed and Tool Pin Profiles. : 537–542.

Vilaça, P., Pépe, N. & Quintino, L. 2006. Metallurgical and corrosion features of friction stir welding of AA5083-H111. *Welding in the World*, 50(9–10): 55–64.

Welding, F.S. 2015. پژوهش‌های آزمایشگاهی (Friction Stir Welding) بر روی آلومینوم 6082-T6. *مجله علمی پژوهشی مهندسی صنایع*, (March): 343–344.

Yazdipour, A. & Heidarzadeh, A. 2016. Effect of friction stir welding on microstructure and mechanical properties of dissimilar Al 5083-H321 and 316L stainless steel alloy joints. *Journal of Alloys and Compounds*, 680: 595–603.

Zareie Rajani, H. R.; Esmaeili, A.; Mohammadi, M.; Sharbati, M.; Givi, M. K. B. (21 February 2012). "The role of Metal-Matrix Composite development During Friction Stir Welding of Aluminum to Brass in Weld Characteristics". *Journal of Materials Engineering and Performance*. 21 (11): 2429–2437.

Zhang, L. & Wang, X. 2018. Microstructure Evolution and Properties of Friction Stir Welding Joint for 6082-T6 Aluminum Alloy. *Materials Research*, 21(6).